Gondwana Research 129 (2024) 201–219

Contents lists available at ScienceDirect

Gondwana Research

journal homepage: www.elsevier.com/locate/gr

Transition from orogenic-like to anorogenic magmatism in the Southern Alps during the Early Mesozoic: Evidence from elemental and Nd-Sr-Hf-Pb isotope geochemistry of alkali-rich dykes from the Finero Phlogopite Peridotite, Ivrea–Verbano Zone

Abimbola C. Ogunyele [a,b,*], Mattia Bonazzi [b], Tommaso Giovanardi [c], Maurizio Mazzucchelli [b,c], Vincent J.M. Salters [d], Alessandro Decarlis [e], Alessio Sanfilippo [a,b], Alberto Zanetti [b]

[a] Department of Earth and Environmental Sciences, University of Pavia, Via Ferrata 1, 27100 Pavia, Italy
[b] CNR – Istituto Geoscienze e Georisorse, Via Ferrata 1, 27100 Pavia, Italy
[c] Department of Chemical and Geological Sciences, University of Modena and Reggio Emilia, Via Campi 103, 41125 Modena, Italy
[d] National High Magnetic Field Laboratory, Department of Earth, Ocean and Atmospheric Sciences, Florida State University, Tallahassee, FL 32310, USA
[e] RICH Center, Earth Sciences Department, Khalifa University of Science and Technology, P.O. Box 12788, Abu Dhabi, United Arab Emirates

ARTICLE INFO

Article history:
Received 8 June 2023
Revised 11 December 2023
Accepted 23 December 2023
Available online 29 December 2023
Handling Editor: Taras Gerya

Keywords:
Alkali-rich dyke swarms
Early Mesozoic magmatism
Finero Phlogopite Peridotite
Subcontinental Lithospheric Mantle
Asthenospheric upwelling
Ivrea-Verbano Zone

ABSTRACT

The Ivrea-Verbano Zone (IVZ) in the westernmost sector of the Southern Alps is an iconic upper mantle to lower continental crust sequence of the Adriatic Plate and provides a geological window into the tectono-magmatic events that occurred at the Gondwana–Laurussia boundary from Late Paleozoic to Early Mesozoic. In this work, we document new geochemical and Nd-Sr-Hf-Pb isotopic data for Early Mesozoic alkali-rich dyke swarms which intruded the Finero Phlogopite Peridotite (northern IVZ) to provide geological constraints on the nature, origin and evolution of Early Mesozoic magmatism in the Southern Alps. The studied dykes are amphibole-phlogopite-bearing and show geochemical features varying between two end-member groups. A dyke group is characterized by HFSE-poor, Al-rich amphibole (Al_2O_3 up to 16 wt%) with high LILE and LREE contents, high radiogenic $^{87}Sr/^{86}Sr_{(i)}$ (0.704732 to 0.704934) and low radiogenic Nd isotopes ($\varepsilon Nd_{(i)}$ from −0.1 to −0.7), which support the occurrence of significant amounts of recycled continental crust components in the parental mantle melts and impart an overall "orogenic-like" affinity. This dyke group was largely derived from metasomatized lithospheric mantle sources. The second group is HFSE-rich with Al-poorer amphibole enriched in LILE and LREE, low radiogenic $^{87}Sr/^{86}Sr_{(i)}$ (0.703761–0.704103) and higher radiogenic Nd isotopes ($\varepsilon Nd_{(i)}$ from +3.4 to +5.4) pointing to an "anorogenic" alkaline affinity and asthenospheric to deep lithospheric mantle sources. Some dykes show both orogenic and anorogenic affinities, providing evidence that the orogenic-like magmatism in the IVZ predates the alkaline anorogenic magmatism. The Finero dyke swarms therefore record a geochemical change of the Early Mesozoic magmatism of the Southern Alps from orogenic-like magmatism, typical of post-collisional settings, to anorogenic alkaline magmatism, common in intraplate to extensional settings, and places a temporal correlation of Early Mesozoic magmatism in the IVZ to those in the eastern and central sectors of the Southern Alps.

1. Introduction

The geodynamic processes that trigger a shift from orogenic-like calc-alkaline magmatism to alkaline OIB-like magmatism in syn- to post-collisional settings are enigmatic, ranging from asthenospheric upwelling to lithospheric delamination, mantle plumes, plume-arc interaction, slab roll-back, slab tearing, and incorporation of exotic enriched mantle components, etc (Marquez et al., 1999; Agostini et al., 2007; Handy et al., 2019; Deng et al., 2023). Such a shift and processes are well-documented in several localities around the Alpine-Mediterranean region and in most subduction zones worldwide (e.g., Coltorti et al., 2007; Agostini et al., 2007; Harangi et al., 2007; Lustrino et al., 2013; Zheng, 2019; Deng et al., 2023). One of such areas in the Alpine-Mediterranean region is the Southern

* Corresponding author.
E-mail address: abimbola.ogunyele01@universitadipavia.it (A.C. Ogunyele).

https://doi.org/10.1016/j.gr.2023.12.011
1342-937X/

Alps where significant magmatic activities occurred during the Late Paleozoic to Early Mesozoic, particularly from the Middle to Late Triassic (ca. 243–237 Ma) (Lustrino et al., 2019; Storck et al., 2019; De Min et al., 2020; Casetta et al., 2021). Petrological and geochemical studies focused on the Middle Triassic volcano-plutonic sequences emplaced at shallow crustal depths and erupted at the surface in the eastern (e.g. Dolomites) and central (Brescian Prealps) sectors of the Southern Alps confirm a K-rich calc-alkaline to shoshonitic affinity of the uprising melts, commonly interpreted as the result of the partial melting of mantle sources presumably subduction-modified during the "Variscan cycle" with negligible crustal contamination (e.g., Lustrino et al., 2019; De Min et al., 2020; Casetta et al., 2021; Nardini et al., 2022). In this case, "Variscan" is used in the broadest sense of the term. In the Late Triassic, the subduction-related magmatism was followed by alkaline OIB-type magmatism represented by the ca. 219 Ma alkaline lamprophyre dykes in the Dolomites (Casetta et al., 2019) and the ca. 217 Ma transitional basaltic dykes in the Brescian Prealps (Cassinis et al., 2008) indicating a significant variation of the mantle sources and geodynamic environment subsequently leading to the opening of the Alpine Tethys during the Lower Jurassic (Cassinis et al., 2008; Casetta et al., 2019).

The opportunity of characterizing different cycles of Early Mesozoic magmatism, their source changes and relationship with the evolution of the geodynamic environment is also possible in the westernmost sector of the Southern Alps in the Ivrea-Verbano Zone (IVZ). The IVZ forms a spectacular exposure of lower to middle continental crust with the widespread occurrence of mantle peridotite lenses (Fig. 1) that provides a unique natural laboratory to study deep crustal and mantle rocks of Late Paleozoic to Early Mesozoic age. The petrochemical record of Triassic–Jurassic magmatism in the IVZ was only recently recognized, and it is particularly relevant in the Finero Complex. The IVZ Triassic–Jurassic magmatism is recorded by a variety of intrusive bodies (mainly veins, dykes and pods) emplaced into the lower crust and mantle peridotites (Stähle et al., 1990; 2001; Grieco et al., 2001; Mazzucchelli et al., 2010; Zanetti et al., 2013; Schaltegger et al., 2015; Denyszyn et al., 2018; Galli et al., 2019; Bonazzi et al., 2020; Giovanardi et al., 2013, 2020; Decarlis et al., 2023). Tuffitic horizons within carbonate platform sequences close to IVZ and some mafic dykes in the adjacent Serie dei Laghi (Zurbriggen, 1996; Handy et al., 1999) also provide evidence of Early Mesozoic magmatism in the westernmost Southern Alps.

However, the Mesozoic magmatism in the Finero Complex and the IVZ at large is still poorly constrained due to the intrinsic complication of its poly-phasic emplacement that occurred between two major orogenic cycles (i.e. the demise of the Variscan belt and onset of the Alpine Tethys). In addition, Mesozoic melts migration started when the Finero Complex was still placed at P-T conditions typical of a continental crust-mantle transition (~1 GPa) and this promoted the re-opening of the geochronological clocks widening time interval brackets of absolute dating (Zanetti et al., 2016). Previous geochemical studies on the Early Mesozoic magmatism of the IVZ point to the variable geochemical signatures of the parental mantle melts from tholeiitic to OIB affinity, often containing continental crustal components (e.g., Giovanardi et al., 2020). Unlike the magmatisms in the Brescian Prealps and Dolomitic areas, the IVZ Triassic magmatism is mostly younger than 235 Ma, providing a unique opportunity to better characterize the Late Triassic tectono-magmatic cycle below or at crust-mantle transition depths. Moreover, the Mesozoic intrusive bodies emplaced in the IVZ mainly show limited interaction with the continental crust. As a consequence, they preserve the primary geochemical features, which allow to provide straightforward constraints on their mantle source compositions.

Here, we present the geochemistry of Early Mesozoic dyke swarms cross-cutting the Finero Phlogopite Peridotite in northern IVZ to: (i) study the origin and evolution of mantle melts and the role of continental crust recycling, highlighting the heterogeneity of the subcontinental lithospheric mantle beneath the Southern Alps, and (ii) to further understand the nature of Triassic–Jurassic magmatism in the Southern Alps tectonic context in the light of the existing literature.

2. Geological settings of the Ivrea-Verbano Zone and Finero Complex

The Ivrea-Verbano Zone (IVZ) is the westernmost sector of the Southern Alps and represents a continuously exposed section of lower to intermediate continental crust (Schmid, 1993; Zanetti et al., 2013; Decarlis et al., 2023; Fig. 1). The IVZ was part of the Mesozoic continental margin of the Adriatic Plate during the opening of the Alpine Tethys and provides a unique opportunity to investigate the Paleozoic to Mesozoic geodynamic evolution of the Gondwana and Laurasia boundary from a lower continental crust perspective (Stampfli and Borel, 2002, 2004; Handy et al., 2010). The present-day exposure of the IVZ results from a 90-degree tilting generated by a series of deformation events that likely started during Permian-Triassic stages of lithospheric thinning in the Variscan post-collisional realm. Pronounced exhumation and blocks rotation took place during the opening of the Jurassic Alpine Tethys (Decarlis et al., 2023 and references therein) and concluded with the Alpine collision (Handy et al., 1999).

The IVZ comprises three main units: (i) the Kinzigite Formation, (ii) the Mafic Complex and (iii) the Mantle Peridotites. The Kinzigite Formation is an amphibolite- to granulite-facies volcano-sedimentary succession underplated and intruded by the *trans*-crustal Mafic Complex during the late Carboniferous-early Permian (Peressini et al., 2007). The Mafic Complex represents a large magmatic system that progressively grew due to a continued input of new magmas. The Valsesia area roughly corresponds to the major axis of the magmatic chamber, reaching a maximum thickness of about 11 km. Several orogenic mantle peridotite bodies line up along the NW margin of the Mafic Complex and parallel to the Insubric Line. The largest and more famous of the Ivrea-Verbano mantle peridotites are, from south to north, the Baldissero, Balmuccia, Premosello and Finero massifs (Fig. 1).

The Finero Complex lies in the northernmost segment of the IVZ (Fig. 1a-b). It is a large (12 x 3 km), lens-shaped succession including a mantle peridotite (the Finero Phlogopite Peridotite; FPP) at the centre surrounded by a layered gabbroic to ultramafic body (the Finero Mafic Complex; FMC). The Finero Complex is bordered by the Insubric Line to the N-NW and by the Kinzigite Formation to the S-SE (e.g. Zanetti et al., 1999; 2013). The FPP is a pervasively metasomatized harzburgitic body (roughly 11 x 1 km) characterized by the widespread occurrence of amphibole and phlogopite (see Decarlis et al., 2023 for an overview). The FMC can be subdivided into three units, from base to top: (1) the Internal Gabbro, overlying the FPP; (2) the Amphibole Peridotite; and (3) the External Gabbro (Siena and Coltorti, 1989). The Internal Gabbro, also called Layered Internal Zone, is ~ 70–120 m thick and mainly consists of garnet-bearing hornblendite with subordinate garnet-bearing amphibole gabbro, anorthosite, pyroxenite and peridotite. The Amphibole Peridotite unit is ~ 400 m thick and is constituted by amphibole-bearing cumulus peridotite (dunite, wehrlite and subordinately lherzolite), pyroxenite and hornblendite. The External Gabbro unit is ~ 400–500 m thick and mainly consists of amphibole gabbro and diorite, with minor pyroxenite and anorthosite bands. The contact between the Amphibole Peridotite and

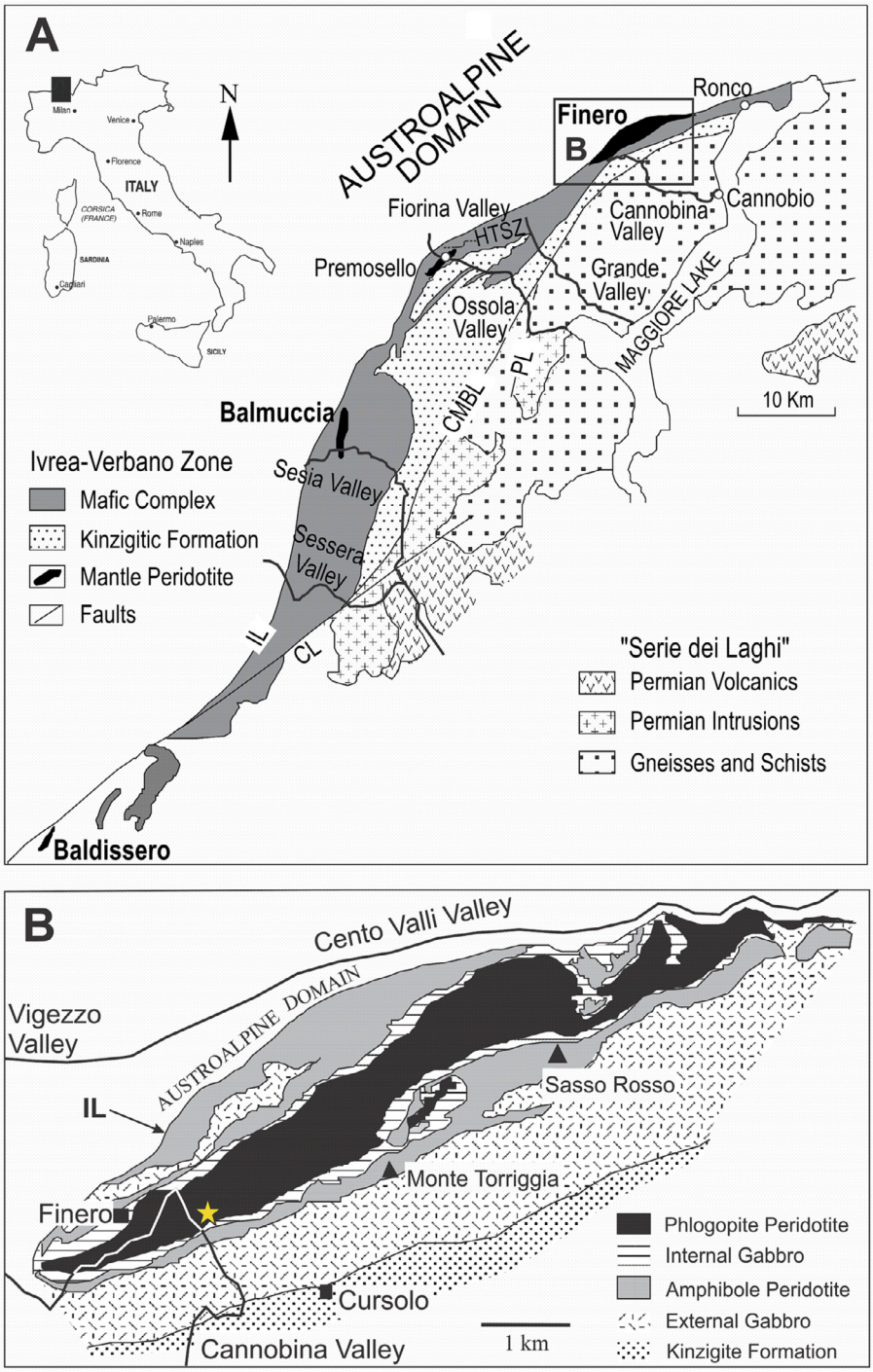

Fig. 1. Geological maps of (a) the Ivrea-Verbano Zone and (b) the Finero Complex with sampling location (yellow star) of the studied dykes around Rio Creves. IL – Insubric Line, CMBL – Cossato-Mergozzo-Brissago Line, PL – Pogallo Line (after Zanetti et al., 1999).

External Gabbro is tectonic (Langone et al., 2018). Many discordant dyke swarms of ultramafic to felsic compositions intrude the FPP and the FMC (Stähle et al., 1990; 2001; Giovanardi et al., 2013, 2020; Grieco et al., 2001; Schaltegger et al., 2015; Langone et al., 2017), some of which are the subject of the present investigation.

3. Field relationships, samples and petrography

The dyke swarms studied in this work are well-exposed in and around a quarry located along the right flank of the Rio Creves, near the contact between the FPP and the FMC (46°06′27.90″N; 8°32′38.76″E; Fig. 1b). The outcrops of the dykes are tens to hundreds of meters far from the outcrops of the sapphirine-bearing gabbroic dykes investigated by Giovanardi et al., (2013, 2020), and few hundreds of meters from the outcrops of mantle peridotite intruded by phlogopite-bearing websterites studied by Zanetti et al. (1999).

Most of the alkali-rich dykes of this study cross-cut at a high angle and show sharp contacts with the Paleozoic mantle foliation of the FPP (frequently at right angle; e.g., Fig. 2a), similar to what is observed for the sapphirine-bearing gabbroic dykes (Giovanardi et al., 2013, 2020). Some alkali-rich dykes are found in shear zones, with sub-parallel to discordant strike to the mantle foliation and

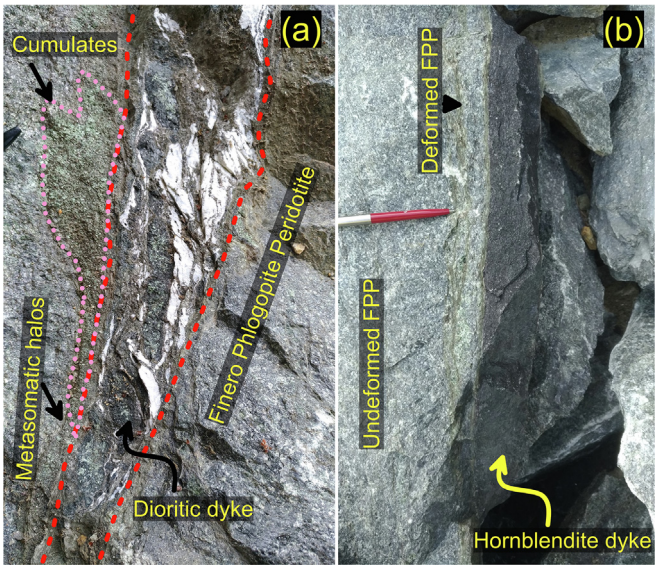

Fig. 2. Field aspects of alkali-rich dykes cross-cutting the host rock, a phlogopite peridotite in Finero, Ivrea-Verbano Zone. (a) Dioritic dyke in which the magmatic structure has been highly deformed by syn-magmatic volatile-driven overpressure in the conduit; and (b) hornblendite dyke within a shear zone which underwent multistage evolution.

testify to a multistage evolution (e.g., Fig. 2b; Corvò et al., 2020). The dykes show extremely variable composition and they are best classified based on their geochemistry. Hence, due to the occurrence of amphibole in all the dyke samples and the variable contents of the High Field Strength Elements (particularly Nb and Ta) in this mineral phase, the studied dykes are categorized into three groups: (1) HFSE-rich dyke group; (2) HFSE-poor dyke group; and (3) composite HFSE-poor and -rich dyke group (Table 1).

3.1. HFSE-rich (HR) dyke group

Dykes of the HR group contain amphibole with high HFSE content (e.g., Nb > 70 ppm). They consist of diorite, albite-dominated anorthosite and hornblendite (Fig. 3). The diorites (samples FI1603, FI1604, FI1605, FI2102, FI2103, FI2104 and FI2105) show variable proportion (~10–40 vol%) of leucocratic patches/layers associated with melanocratic segregates. They cross-cut the host peridotite foliation and show a magmatic structure often deformed by *syn*-magmatic volatile-driven overpressure that took place in the conduits (Fig. 2a). The texture is variable but commonly porphyroclastic, with magmatic domains and fine-grained mosaic textures (Fig. 4a-f). Mafic phases in the melanocratic layers of the diorites range from ~ 90 vol% amphibole to ~ 90 vol% phlogopite. Amphiboles are commonly green to brown, locally fractured and filled by fine-grained phlogopite, plagioclase, apatite, Nb-Ta oxides and calcite. Leucocratic patches formed by plagioclase and apatite show evidence of plastic flow, rotation and grinding. The melanocratic parts locally contain clinopyroxenite cumulates (Fig. 3b).

Anorthosites (samples FI19A01, FI19A02 and FI19A04) are essentially composed of albite (>90 vol%) and oligoclase with subordinate brown amphibole, phlogopite and apatite. Zircon, titanite, allanite, calcite and Nb-Ta oxides are common accessory minerals. The texture is hypidiomorphic to glomerophyric (Fig. S1 in Supplementary Information). HFSE-rich hornblendites (samples FI1501 and FI1612; Fig. 3) are almost wholly composed of brown amphibole (>90 vol%) with hypidiomorphic texture that locally contains thin layers and/or pods of olivine, clinopyroxene, sulphides, and phlogopite. Phlogopite, apatite, Nb-Ta oxides and calcite are subordinate (Fig. S2 in Supplementary Information). U-Pb dating of zircons from some HR dioritic and anorthosite dykes show wide age intervals ranging from 221 ± 9 Ma to 192 ± 8 Ma with peak concordant ages around 200 Ma (Ogunyele et al., 2021; Bonazzi et al., 2022).

3.2. HFSE-poor (HP) dyke group

Dykes of the HP group are characterized by amphibole with low contents of HFSE (e.g., Nb < 9 ppm). They include hornblendite (FI1608) and gabbro (FI2101), both of which outcrop in shear zones within the host peridotite. The hornblendite is a mylonitic to ultramylonitic rock almost entirely composed of fine to very fine amphiboles (Fig. 5a). It is formed by a peculiar alternation of fine-grained amphibole and olivine-rich horizons sandwiched between mylonitic amphibole layers. Phlogopite, apatite and sulphide occur as accessories. The gabbro is similar in structure and

Table 1
Description of selected samples of Finero dykes and analytical methods of investigation.

Sample ID	Rock type	Grouping	Major mineral phases	Textures	SEM-EDS	EMPA	LA-ICP-MS	Nd-Sr-Hf-Pb isotopes on Amph
FI1603	Diorite	HFSE-rich	Amph + Pl + Phl + Ap + (Cpx)	Magmatic to porphyroclastic	X	X	X	X
FI1604	Diorite	HFSE-rich			X	X	X	
FI1605	Diorite	HFSE-rich			X	X	X	
FI2102	Diorite	HFSE-rich			X	X	X	
FI2103	Diorite	HFSE-rich				X	X	X
FI2104	Diorite	HFSE-rich				X	X	
FI2105	Diorite	HFSE-rich			X	X	X	
FI1501	Hornblendite (with olivine layer)	HFSE-rich	Amph + Phl + Ap + (Ol)	Hypidiomorphic	X	X	X	X
FI1612	Hornblendite	HFSE-rich	Amph + Phl + Ap + (Cpx)			X	X	
FI19A01	Albite-dominated anorthosite	HFSE-rich	Pl + Ap ± Amph ± Phl	Hypidiomorphic to glomerophyric			X	
FI19A02	Albite-dominated anorthosite	HFSE-rich			X	X	X	
FI19A04	Albite-dominated anorthosite	HFSE-rich			X	X	X	
FI1608	Hornblendite	HFSE-poor	Amph + Phl + Ap	Mylonitic to ultramylonitic	X	X	X	
FI2101	Gabbro bordered by orthopyroxenite	HFSE-poor	Amph + Phl + Ap + (Opx)	Banded		X	X	X
FI2106	Diorite	Composite	Amph + Pl + Phl + Ap	Porphyroclastic	X	X	X	
FI1607	Hornblendite dyke with cumulus peridotite	HFSE-poor and -rich	Amph + Phl + Ap + (Ol)	Porphyroclastic	X	X	X	X

*Phases in brackets are minerals present in cumulates associated with the dykes (mineral abbreviations after Kretz, 1983).

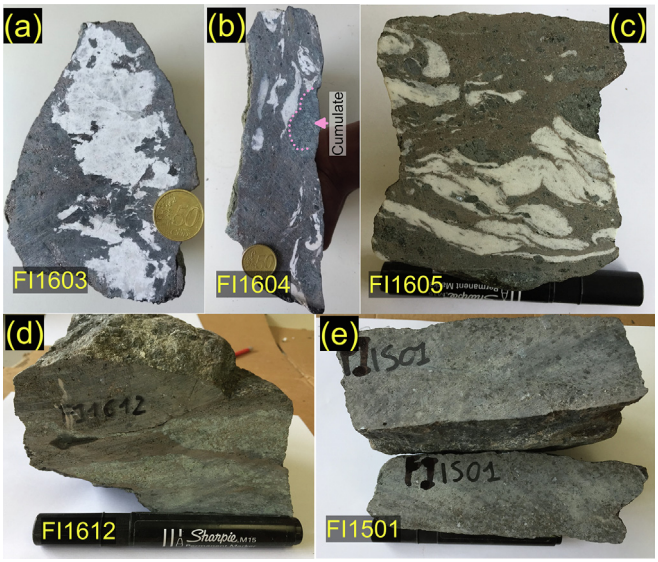

Fig. 3. Mesoscopic aspects of the Finero HFSE-rich dykes. (a, b, c) HFSE-rich dioritic dyke samples showing leucocratic patches/layers associated with ultramafic segregates and xenoliths of cumulus clinopyroxenite; (d, e) HFSE-rich hornblendite dyke samples. Cumulus clinopyroxenites is also present in the hornblendite dyke sample FI1612.

mineralogy to sapphirine-bearing gabbroic dykes studied by Giovanardi et al., (2013, 2020). It consists of outer orthopyroxene layers bordering internal layers of brown to greenish amphiboles and plagioclase (Fig. 5b). Phlogopite, apatite, sapphirine, spinel, and calcite are present. Zircon is however absent in both samples.

3.3. Composite HFSE-poor and -rich (HC) dyke group

Dykes belonging to the HC group contain amphiboles ranging from HFSE-poor to HFSE-rich compositions. The two sampled dykes are a diorite (sample FI2106) and a hornblendite with cumulus peridotite (FI1607), both outcropping in shear zones. The diorite (FI2106) is a porphyroclastic amphibole-dominated rock cut by leucocratic layers of plagioclase and apatite. Phlogopite, sulphides and calcite occur as accessories in the dyke (Fig. 6). Amphibole in the central part of the dyke is enriched in HFSE and grades to HFSE-poor composition towards the margins, suggesting that an HFSE-poor dyke was intruded and overprinted by HFSE-rich melt (s). This observation is crucial to assess the relative timing of HFSE-rich and HFSE-poor dykes' emplacement, as field cross-cutting relationships are missing at present and zircons are absent in the HFSE-poor dykes.

Sample FI1607 is composed of a 3 cm thick cumulus peridotite layer and a 20 cm thick porphyroclastic hornblendite (Fig. S3 in Supplementary Information). The latter is formed by brown amphibole, phlogopite, apatite, calcite and sulphides. Interstitial clino- and orthopyroxene, probably resulting from the dehydration of amphibole at high PT conditions are present. Veinlets of brown amphibole also occur within the porphyroclastic cumulus olivine-dominated peridotite.

4. Analytical methods

Petrographic features and mineral assemblages of the dyke samples were assessed by polarized light microscopes and SEM-EDS at Dipartimento di Scienze della Terra e dell'Ambiente (DSTA), University of Pavia, and at Dipartimento di Scienze Chimiche e Geologiche (DSCG), University of Modena and Reggio Emilia. The SEM-EDS at DSTA UNIPV comprises a Tescan Mira3 XMU-series FESEM equipped with an EDAX-EDX operated at an accelerating voltage of 20 kV, beam intensity of 16.5nA, spot area of 100 × 100 μm, counts of 100 s., and a working distance of 15.8 mm. Data were processed with EDAX Genesis software using the ZAF algorithms.

Mineral major element compositions were measured by electronprobe microanalysis with a JEOL JXA-8200 Superprobe equipped with five WDS spectrometers operating in wavelength dispersive mode, housed at Dipartimento di Scienze della Terra "Ardito Desio", University of Milano. Operating conditions were 15 kV accelerating voltage, 15nA beam current, 1–5 μm spot size, and a counting time of 30 s on the peaks and 10 s on the backgrounds. Natural minerals (olivine for Mg; omphacite for Na; ilmenite for Ti; rhodonite for Mn; K-feldspar for K; anorthite for Al and Ca; wollastonite for Si; fayalite for Fe and niccolite for Ni) and synthetic chromite were used as standards. The results were corrected for matrix effects using the conventional ZAF method provided by the JEOL software package. Results are considered to be accurate within 2–6 %.

Trace element contents of mineral phases (amphibole, phlogopite, plagioclase, apatite, pyroxenes and olivine) in thin sections and separates of the dyke samples were determined with LA-ICP-MS housed at Centro Interdipartimentale Grandi Strumenti (CIGS) of the University of Modena and Reggio Emilia and at Istituto di Geoscienze e Georisorse, Consiglio Nazionale delle Ricerche, Sede Secondaria di Pavia (IGG-CNR Pavia). The instrument at the CIGS consists of an ICP-MS X Series II (ThermoFisher Scientific) coupled to a 213 nm Nd:YAG laser ablation system (New Wave Research™). The ICP-MS was tuned using NIST SRM 612 synthetic glass standard to optimize the signal intensity and stability, monitoring ^{139}La, ^{238}U and the ^{232}Th/^{248}ThO ratio. NIST SRM 614, NIST SRM 612 and NIST SRM 610 were used as external standards during the analytical session. Data reduction was performed using the PlasmaLab software. LA-ICP-MS at the IGG-CNR Pavia coupled a 213 or 266 nm Nd:YAG laser ablation system (Quentel™) to a Triple-quadrupole ICP-MS system (Agilent™ Series 8900). The ICP-MS was tuned using NIST SRM 610 synthetic glass to optimize the signal intensity and stability and remove molecular interferences by monitoring ^{24}Mg, ^{115}In, ^{238}U and the ^{232}Th/^{248}ThO ratio. Data reduction was done with the GLITTER software (Griffin et al., 2008). NIST SRM 610 was used as external standard and USGS reference sample BCR2g was used as unknown. The laser was operated with a 10 Hz repetition rate, 10 J/cm^2 fluence and 50–60 μm spot size. ^{44}Ca was used as an internal standard for amphibole, apatite, and clinopyroxene; and ^{29}Si for plagioclase, phlogopite, orthopyroxene and olivine. Precision and accuracy are at ± 5 % and ± 10 %, respectively.

Nd, Hf, Sr and Pb isotopes measurements were performed on amphiboles separated from three HFSE-rich samples [FI1603, FI2103 (diorites), FI1501 (hornblendite)], one HFSE-poor gabbro (FI2101) and one composite dyke (i.e. the HFSE-poor amphiboles of hornblendite dyke FI1607). About 100 mg of amphibole separate for each sample was leached, dissolved, processed through ion exchange columns and measured for isotopes at the National High Magnetic Field Laboratory, Florida State University. The separates were leached in 5 ml 2.5 N HCl and < 30 % H_2O_2 for 60 min at room temperature to remove any alteration products. The leached separates were rinsed several times with quartz sub-boiling distilled water. Subsequent dissolution and column chemistry was performed after procedures described by Stracke et al. (2003) and Woelki et al. (2023). Sr isotope compositions were measured by thermal ionization mass spectrometry (TIMS) using a Finnigan MAT 262 RPQ system. The ^{87}Sr/^{86}Sr ratios are corrected for mass bias using a ^{88}Sr/^{86}Sr value of 0.1194 and reported relative to the E&A $SrCO_3$ standard of ^{87}Sr/^{86}Sr of 0.708000. Blanks for Sr were less than 100 pg. Nd, Hf and Pb isotopes were measured using a

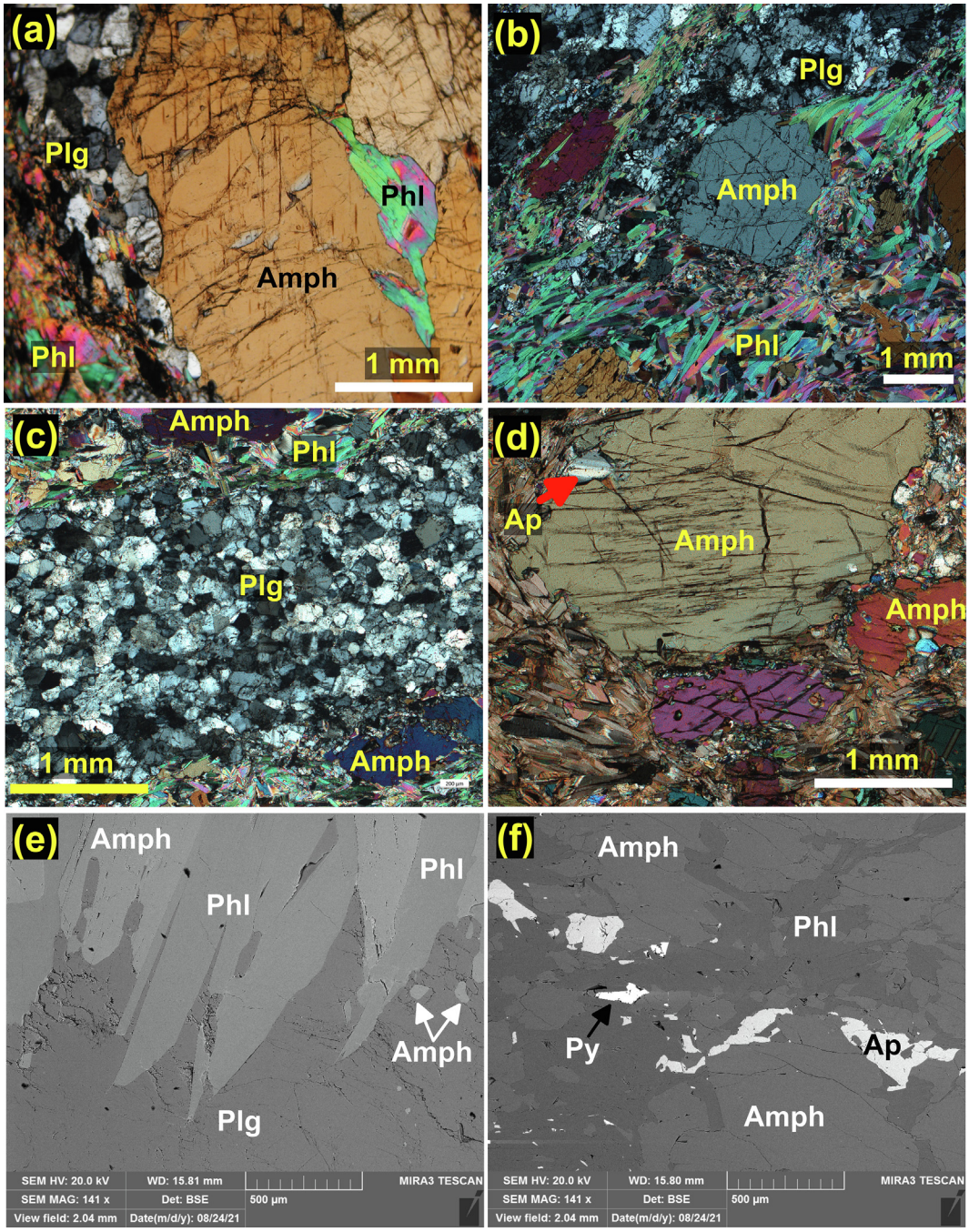

Fig. 4. Microscopic aspects of the Finero HFSE-rich dioritic dykes. Photomicrographs showing (a) large magmatic amphiboles within plagioclase and fine-grained phlogopite. The amphibole contains fractures filled by phlogopite, plagioclase and apatite; (b) amphibole porphyroclasts embedded within a groundmass of fine-grained phlogopite, amphibole and plagioclase; (c) leucocratic layer of medium- to fine-grained plagioclase and apatite within melanocratic layers made by amphibole porphyroclasts and fine-grained phlogopite; (d) amphibole porphyroclasts containing apatite wrapped around by fine-grained phlogopite and plagioclase; (e) BSE image showing plagioclase "permeating" amphibole + phlogopite layer; and (f) BSE image showing the interstices of amphiboles filled by phlogopite, apatite and pyrite.

ThermoFisher Neptune Multi-Collector ICP-MS system. The $^{143}Nd/^{144}Nd$ ratios are corrected for mass bias using a $^{146}Nd/^{144}Nd$ ratio of 0.7219 and are reported relative to the La Jolla standard of 0.511850. Blanks for Nd were less than 10 pg. The $^{176}Hf/^{177}Hf$ ratios are corrected for mass bias using a $^{179}Hf/^{177}$-Hf ratio of 0.7325 and reported relative to the JMC-475 value of ^{176}-$Hf/^{177}Hf$ = 0.282150. Blanks for Hf were less than 40 pg. The Pb isotope measurements were normalized to NBS 981 values of ^{206}-$Pb/^{204}Pb$, $^{207}Pb/^{204}Pb$, and $^{208}Pb/^{204}Pb$ ratios of 16.9356, 15.4891, and 36.7006, respectively. Blanks for Pb were less than 30 pg. The reproducibility of the E&A, LaJolla, JMC475 and NBS 981 standards is similar to their in-run precision.

5. Analytical results

5.1. Mineral major element composition

The full dataset of major and minor elements in mineral phases from the studied dyke samples including each mineral analysis is reported in Supplementary Table 1.

5.1.1. Amphibole

Following the normalization scheme of Ridolfi et al. (2018) and the classification scheme of Hawthorne et al. (2012), amphiboles are pargasites in all the HR, HP and HC group samples (Fig. 7). Amphiboles from the HR dyke group (diorites and associated clinopyroxenite cumulates, hornblendites and anorthosites) are characterized by magnesium numbers (Mg# = molar [Mg/(Mg + Fe_t)] * 100) from 73 to 85, and contain 9–13 wt% Al_2O_3, 0.2–2.1 wt% TiO_2, and 0.2–1.4 wt% K_2O.

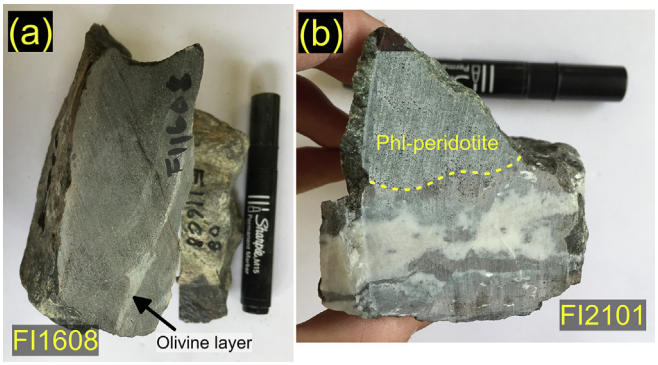

Fig. 5. Mesoscopic aspects of the Finero HFSE-poor dykes. (a) HFSE-poor hornblendite dyke sample showing mylonitic to ultramylonitic texture. In this sample, ultramylonitic amphibole and olivine-rich layers are sandwiched between fine-grained mylonitic amphibole layers. (b) HFSE-poor gabbroic dyke sample with the host phlogopite peridotite. Between the host peridotite and the gabbroic dyke, an orthopyroxenite layer is present.

Amphiboles from the HP dykes are more enriched in Al_2O_3 (13–16 wt%) and TiO_2 (1.3–2.6 wt%), and show contrasting major elements chemistry from the HR dykes. Mg# of amphiboles from the HP hornblendite and gabbro shows significant variations from 63 to 71 and 74 to 88, respectively. K_2O ranges from 0.15 to 0.57 wt %. The composition of amphiboles from the gabbroic dyke is similar to those reported for sapphirine-bearing gabbroic dykes from FPP (Giovanardi et al., 2013, 2020).

In the HC group, amphiboles are Al- and Ti-rich pargasites showing no systematic major element variation between HFSE-rich and HFSE-poor amphiboles. Generally, they contain 13–15 wt% Al_2O_3, 2.1–2.7 wt% TiO_2 and 0.4–0.6 wt% K_2O. The composite diorite dyke (FI2106) contains amphiboles with Mg# from 60 to 64, whereas amphiboles from the composite hornblendite dyke with cumulus peridotite (FI1607) have Mg# varying from 58 to 73.

5.1.2. Plagioclase

In HR dioritic and anorthosite dykes, plagioclase is predominantly albite (An 6–11), as in corundum-bearing felsic dykes from central IVZ (Bonazzi et al., 2020) and nepheline-bearing alkaline dyke from FPP (Stähle et al., 1990). Plagioclase in HP gabbroic dyke, is labradorite to bytownite (An 69–87), similar to what was reported by Giovanardi et al., (2013, 2020) for sapphirine-bearing gabbroic dykes from FPP. Oligoclase (An 23–30) occurs in the HC dioritic dyke (Fig. 8a). Albite and calcite veinlets are found within the oligoclase bands (see Fig. 6e).

5.1.3. Phlogopite

Mica is phlogopite in all the dyke groups (Fig. 8b). Phlogopites from the HR dykes have Mg# from 76 to 89, 13–16 wt% Al_2O_3

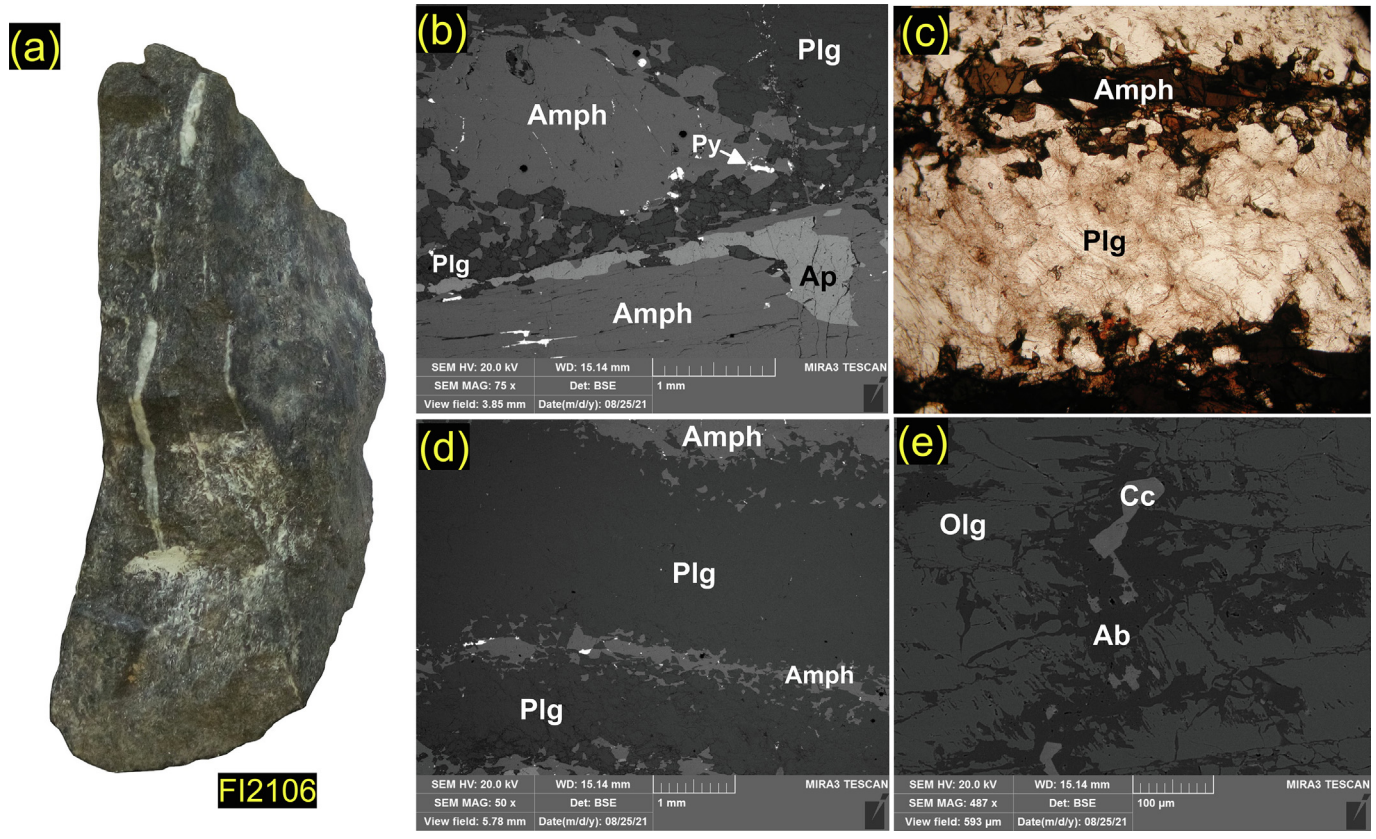

Fig. 6. (a) Representative sample of the Finero composite HFSE-poor and -rich dioritic dyke (FI2106) showing thin leucocratic layers within the melanocratic rock; (b) BSE image of the dyke showing porphyroclasts of amphiboles and plagioclase within a groundmass made by similar minerals and apatite. Apatite appears to vein an amphibole porphyroclast; (c-d) photomicrograph and BSE image showing a leucocratic layer made by plagioclase within amphibole layers. The leucocratic layer is also cut by veinlets of fine-grained amphiboles and sulphides; and (e) BSE image showing albite and calcite veinlets within oligoclase in the dyke.

and 0.3–3.1 wt% TiO_2. Phlogopite is scarce in the HP dykes and was not analyzed for major elements in this study. However, analysis of phlogopites from the sapphirine-bearing gabbroic dykes from FPP by Giovanardi et al., (2013, 2020) showed they contain 16–20 wt % Al_2O_3, 0.6–3.4 wt% TiO_2 and Mg# from 70 to 93.

In the HC dioritic dyke, phlogopite shows high Al_2O_3 (~17 wt%) and TiO_2 (~4 wt%) contents with Mg# between 71 and 73. Phlogopite from the HC hornblendite dyke shows a progressive increase in Mg# passing from the hornblendite (79–81) to the cumulus peridotite (87–88). Al_2O_3 and TiO_2 contents in both domains are similar, ranging from 15 to 17 wt% and 2–4 wt%, respectively.

5.1.4. Apatite

Apatite in the HR dykes is rich in Cl (0.3–3.5 wt%) and locally in F (up to 3.10 wt%) and LREE (La-, Ce-, Nd-oxides). Apatite from the HP hornblendite contains less Cl (~0.6 wt%). In the HC dykes, apatite contains 0.5–1.9 wt% Cl and 1.6–1.9 wt% F.

5.1.5. Pyroxenes

The clinopyroxenite cumulates associated with HR dioritic dykes are composed of diopside with 21–23 wt% CaO, 0.2–0.5 wt % Cr_2O_3, 0.9–2.2 wt% Al_2O_3, <0.1 wt% TiO_2, 7–20 Cr# (Cr# = molar [Cr /(Cr + Al)] * 100) and 84–89 Mg#. Interstitial clinopyroxene of

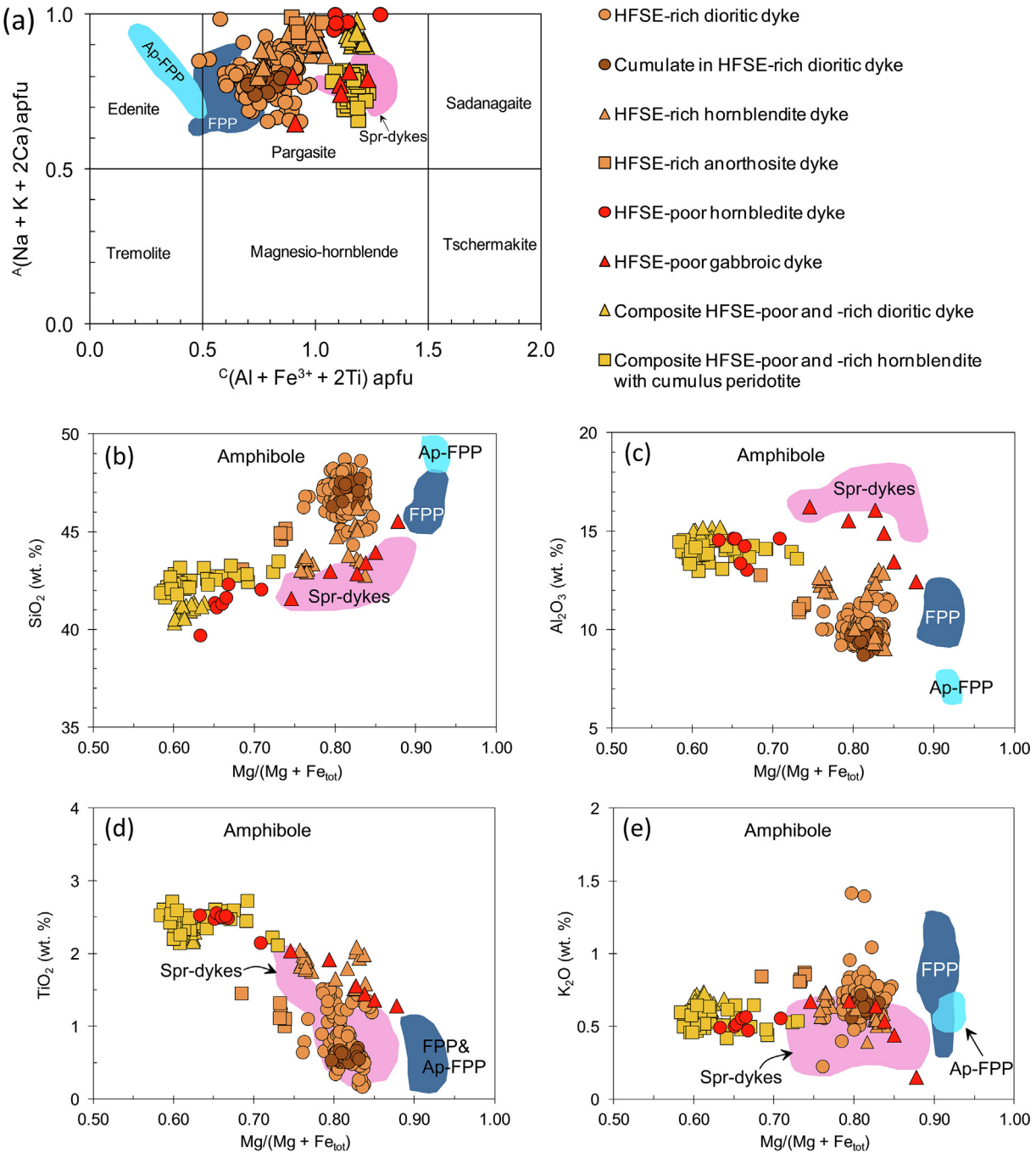

Fig. 7. (a) Classification (after Hawthorne et al., 2012); and (b) major elements discrimination of amphiboles from the alkali-rich dykes of Finero. Plotted literature data are: Finero Phlogopite Peridotite (FPP) and Apatite-bearing Phlogopite Peridotite (Ap-FPP) from Zanetti et al., 1999 and Giovanardi et al., 2020; and sapphirine-bearing gabbroic dykes (Spr-dykes) from Giovanardi et al., 2020.

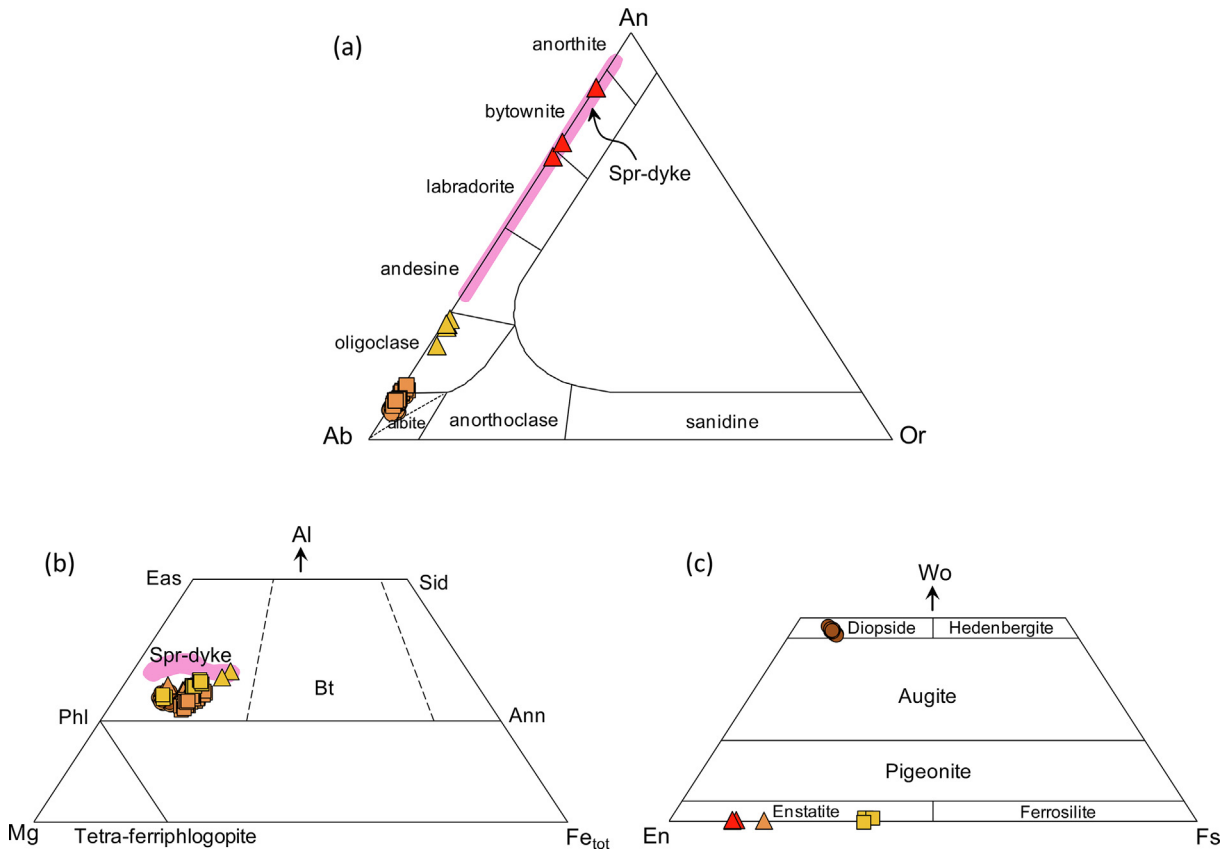

Fig. 8. Classification of (a) plagioclase; (b) phlogopite; and (c) pyroxenes from the alkali-rich dykes of Finero. Sample symbols are as in Fig. 7. Plotted literature data are sapphirine-bearing gabbroic dykes from Giovanardi et al., 2020.

diopside composition and orthopyroxene (enstatite: 62–63; Mg#: 62–64) also occur in the HC hornblendite dyke, probably resulting from dehydration of amphibole rim. Orthopyroxenes from orthopyroxenite layers around the HP gabbroic dyke (FI2101) have enstatite content of 82–88 and Mg# of 83–89 (Fig. 8c).

5.1.6. Olivine

Olivine from the cumulus peridotite (FI1607) and olivine layer in hornblendite (FI1501) shows Fe-enriched composition with forsterite content (Fo = molar [Mg/(Mg + Fe$_t$)] $*$ 100) from 77 to 82.

5.2. Mineral trace element composition

The complete trace element dataset, including each mineral analysis for the three dyke groups is reported in Supplementary Table 2.

5.2.1. Amphibole

Amphiboles from the HR dykes are generally enriched in incompatible trace elements relative to the composition of the primitive mantle (PM, McDonough and Sun, 1995; Fig. 9a-d). The amphiboles from all the HR dyke samples are high in Ba, Rb, Sr, Nb, Ta, Zr, Hf, Ti; low in Th, U and Cs; and show strongly positive anomalies in Nb and Ta, weakly negative to strongly positive anomalies in Zr and Hf, and distinct negative Ti and Pb anomalies on the PM-normalized plot. Amphibole shows L-MREE-enriched CI-normalized patterns, which are almost flat for LREE and HREE with strong fractionation among MREE and a weak positive anomaly in Eu (Eu_N/Eu_N^* = 1.02–1.39; CI chondrite-normalized, Lyubetskaya and Korenaga, 2007). They also show subchondritic Ti/Nb (7–151) and Zr/Nb (0.7–4.1) ratios. The geochemical signature of the amphiboles from samples of the HR group is consistent with amphiboles from intraplate settings (I-Amph) (Moine et al., 2001; Witt-Eickschen et al., 2003; Coltorti et al., 2004, 2007).

Amphiboles from the HP dykes are also enriched in incompatible trace elements (e.g. Ba, Rb, Sr, Pb). However, these samples show contrasting HFSE contents and patterns compared to the amphiboles from the HR dykes. The HP hornblendite and gabbroic dykes are characterized by amphibole showing distinct negative anomalies in Nb, Ta, Zr and Hf with a typical fractionation pattern of $Ba_N > Nb_N > Ta_N$ (Fig. 9e). They also display an L-MREE-enriched convex-upward pattern (Fig. 9f) and relatively lower ΣREE abundances compared to amphiboles from the HR dykes. In contrast to those of the HR dykes, amphibole from the HP dykes shows suprachondritic Ti/Nb (1030–4876) and Zr/Nb (4.3–11.4) ratios typical for suprasubduction settings (S-Amph) (Zanetti et al., 1999; Gregoire et al., 2001; Ishimaru et al., 2007; Coltorti et al., 2007; Zheng, 2019).

The HC dioritic dyke (FI2106) contains amphiboles with HFSE-rich and HFSE-poor compositions. Both amphibole compositions are enriched in incompatible trace elements (e.g. Ba, Rb, Sr, Pb) and show variable Nb, Ta, Zr and Hf contents. The margins of the dyke contain amphibole poor in Nb, Ta, Zr and Hf displaying negative anomalies in these elements, with fractionation patterns of $Ba_N > Nb_N > Ta_N$ and suprachondritic Ti/Nb and Zr/Nb very similar to the amphibole of the HFSE-poor hornblendite and gabbroic dykes. Geochemical analysis on amphibole conducted from the margins to the center of the dyke revealed a progressive increase in the HFSE towards the centre. Amphibole in the central part of the dyke is enriched in Nb, Ta, Zr and Hf showing strongly positive anomalies in these elements, with subchondritic Ti/Nb and Zr/Nb very similar to amphibole from the HFSE-rich dykes (Fig. 10a).

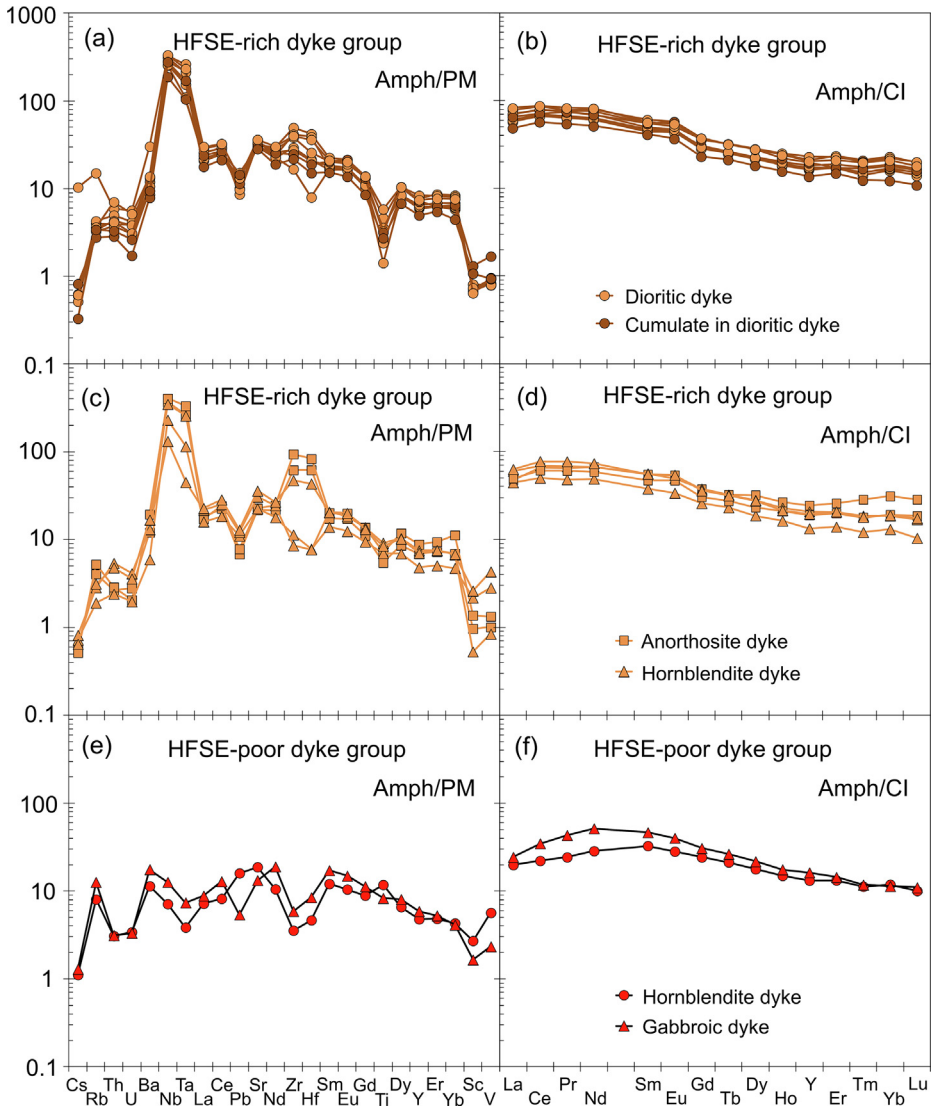

Fig. 9. Incompatible trace elements and REE patterns of amphiboles from (a-b) HFSE-rich dioritic dykes and associated clinopyroxenite cumulates; (c-d) HFSE-rich hornblendite and anorthosite dykes; and (e-f) HFSE-poor hornblendite and gabbroic dykes of Finero. Shown are the compositional averages for each dyke sample. PM and CI-chondrite values are from McDonough and Sun (1995) and Lyubetskaya and Korenaga (2007).

In addition, amphibole shows a geochemical gradient in REE from the margins to the centre where ΣREE abundances are markedly higher (Fig. 10b).

In the composite dyke FI1607, amphibole in hornblendite farther away from the cumulus peridotite shows relatively LILE-, HFSE- and LREE-depleted composition. The LILE, HFSE and REE increase towards the margin with the cumulus peridotite (Fig. 10-c-d). Amphibole veinlets in the cumulus peridotite, however exhibit strongly positive Nb anomaly; a strong decoupling between Nb and Ta; negative Zr, Hf, Ti and Pb anomalies, and highest ΣREE abundances (Fig. 10c-d).

5.2.2. Phlogopite

Similar to amphibole, phlogopites from all HR dykes are strongly enriched in Nb and Ta. Phlogopite from the margin between hornblendite and cumulus peridotite in the composite dyke sample FI1607, however is less enriched in Nb-Ta (Fig. S4 in Supplementary Information). All analyzed phlogopites are enriched in Li, Cs, Rb, Ba, Pb, Sr and Ti; and depleted in Zr, Hf, Th, U, REE, and Sc.

5.2.3. Plagioclase

Albite from all HR diorite and anorthosite dykes is enriched in LREE, strongly depleted in M–HREE (often below the detection limit) and shows the typical strong positive anomaly in Eu. Plagioclase from the HP gabbroic dyke and HC diorite dyke shows similar REE patterns to the HR dykes, but with higher absolute abundances of L-MREE (Fig. S5 in Supplementary Information).

5.2.4. Apatite

Apatite from all dyke groups is characterized by strong enrichments in REE, Th, U, Sr and Pb. In chondrite-normalized patterns, all apatites show strong enrichment in LREE relative to MREE and HREE. Apatite from the HR dykes shows the highest content of REE (Fig. S5 in Supplementary Information).

5.2.5. Pyroxenes

Clinopyroxenes from clinopyroxenite cumulates in HR diorite dykes show trace element contents and patterns that are similar to amphibole in the cumulates and diorites, except for Rb, Ba, Cs, Nb, Ta and Ti, which are strongly depleted, according to crystallochemical constraints. Clinopyroxene from the composite

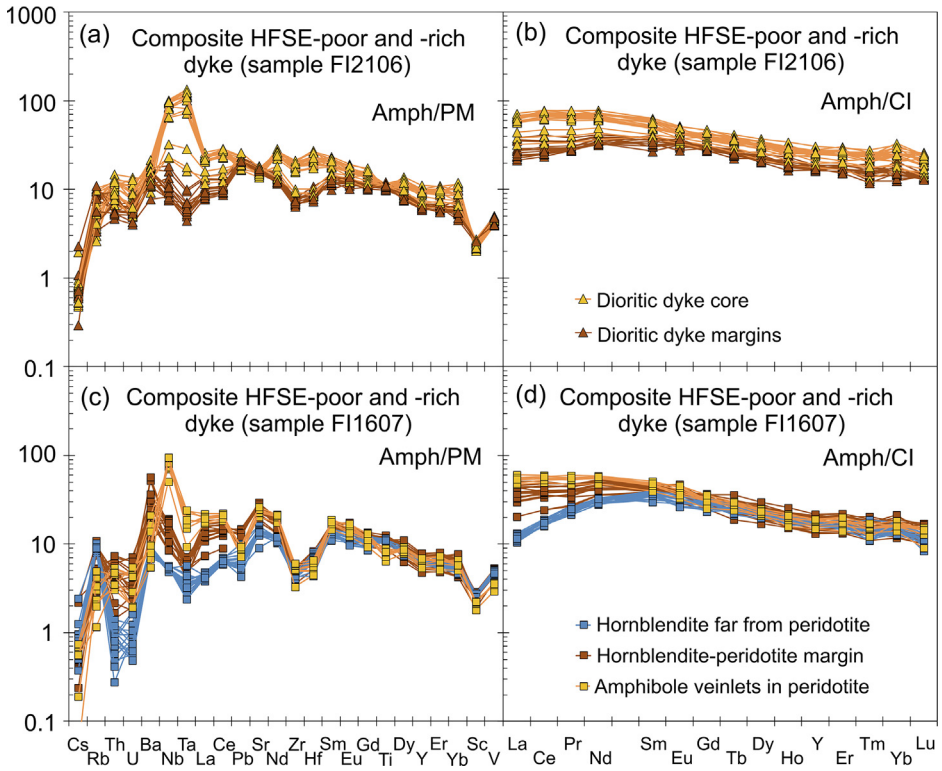

Fig. 10. Incompatible trace elements and REE patterns of amphiboles from (a-b) composite HFSE-poor and -rich dioritic dyke (FI2106); and (c-d) composite HFSE-poor and -rich hornblendite dyke with cumulus peridotite (FI1607) of Finero. Shown are the individual mineral analyses for each dyke sample. PM and CI-chondrite values are from McDonough and Sun (1995) and Lyubetskaya and Korenaga (2007).

hornblendite sample FI1607 shows a convex-upward REE pattern similar to co-existing amphiboles but with lower elemental abundances. Orthopyroxenes show strongly depleted LREE contents relative to M–HREE (Fig. S6 in Supplementary Information).

5.2.6. Olivine

Olivine from the cumulus peridotite (FI1607) and olivine layer in hornblendite (FI1501) is depleted in most trace elements relative to the primitive mantle. Ni, Co and Ti range from 941 to 2076 ppm, 107–145 ppm, and 3–7 ppm, respectively. The low Ni/Co (<20) and Ni/Mn (<2) values are typical of magmatic olivines (Wang et al., 2021).

5.3. Nd-Sr-Hf-Pb isotopes

The measured and initial Nd-Sr-Hf-Pb isotopic compositions of amphibole from selected dyke samples are reported in Supplementary Table 3 and Fig. 11. The initial isotopic ratios of the selected HFSE-rich dyke samples were corrected to 200 Ma in accordance with U-Pb peak ages of zircons from the HFSE-rich diorites and anorthosites (Ogunyele et al., 2021; Bonazzi et al., 2022) and to other published zircon ages of alkaline magmatism in the IVZ straddling the Triassic–Jurassic boundary (e.g., Schaltegger et al., 2015; Galli et al., 2019). The HFSE-poor dyke samples, in the absence of precise emplacement ages, were also corrected to 200 Ma, however, correction using this age results in only minor uncertainties: for example, if an age of 225 Ma were used (similar to the age used by Giovanardi et al., 2020 for the sapphirine-bearing gabbroic dykes), calculated $\varepsilon Nd_{(i)}$, $\varepsilon Sr_{(i)}$, and $\varepsilon Hf_{(i)}$ values would be higher by ~ 0.1, ~0.3 and ~ 0.3, respectively.

Amphibole from the HFSE-rich diorites and hornblendite shows Nd and Sr isotopic compositions significantly different from those of the HFSE-poor dykes. On the Nd-Sr isotopic diagram (Fig. 11a), the HFSE-rich dykes ($\varepsilon Nd_{(i)}$: +3.4 to +5.4; $^{87}Sr/^{86}Sr_{(i)}$: 0.703761 to 0.704103) plot very close to the nepheline-bearing alkaline dykes of FPP and alkaline lamprophyres from Predazzo, Dolomites (Stähle et al., 2001; Casetta et al., 2019) whereas the HFSE-poor dykes ($\varepsilon Nd_{(i)}$: −0.1 to −0.7; $^{87}Sr/^{86}Sr_{(i)}$: 0.704732 to 0.704934) plot within the field of the Middle Triassic magmatic rocks of Dolomites (SATIR in Fig. 11a; Lustrino et al., 2019; Casetta et al., 2021; Nardini et al., 2022). On the Nd-Hf isotopic diagram (Fig. 11b), the two dyke groups plot differently along the Nd-Hf mantle array with the HFSE-rich dykes plotting within the OIB field and the HFSE-poor dykes at the end of the OIB field. Both dyke groups however exhibit similar EMII-like Pb isotopic composition ($^{206}Pb/^{204}Pb$ = 18.4–18.7; $^{207}Pb/^{204}Pb$=~15.6; $^{208}Pb/^{204}Pb$ = 38.4–38.5) (Fig. 11c-d).

6. Discussion

6.1. Multistage and prolonged injection of melts into the subcontinental lithospheric mantle during the Early Mesozoic

Field, petrographic and geochemical evidence suggest that the intrusion of the studied Finero dyke swarms into the host phlogopite peridotite (FPP) occurred as multistage, multiphase and prolonged magmatic events during the Early Mesozoic. The HFSE-rich dykes, in particular the diorite dykes, show clear field and petrographic evidence of multiple melt percolations into their conduits, such as:

(i) Injection of leucocratic layers of plagioclase and apatite into melanocratic segregates of amphibole and phlogopite.

(ii) Small inclusions of melanocratic segregates of mainly amphibole within leucocratic layers.

(iii) Deformation of the original magmatic structure of the dykes by *syn*-magmatic volatile-driven overpressure, probably caused by a high-energy, focused injection of extremely

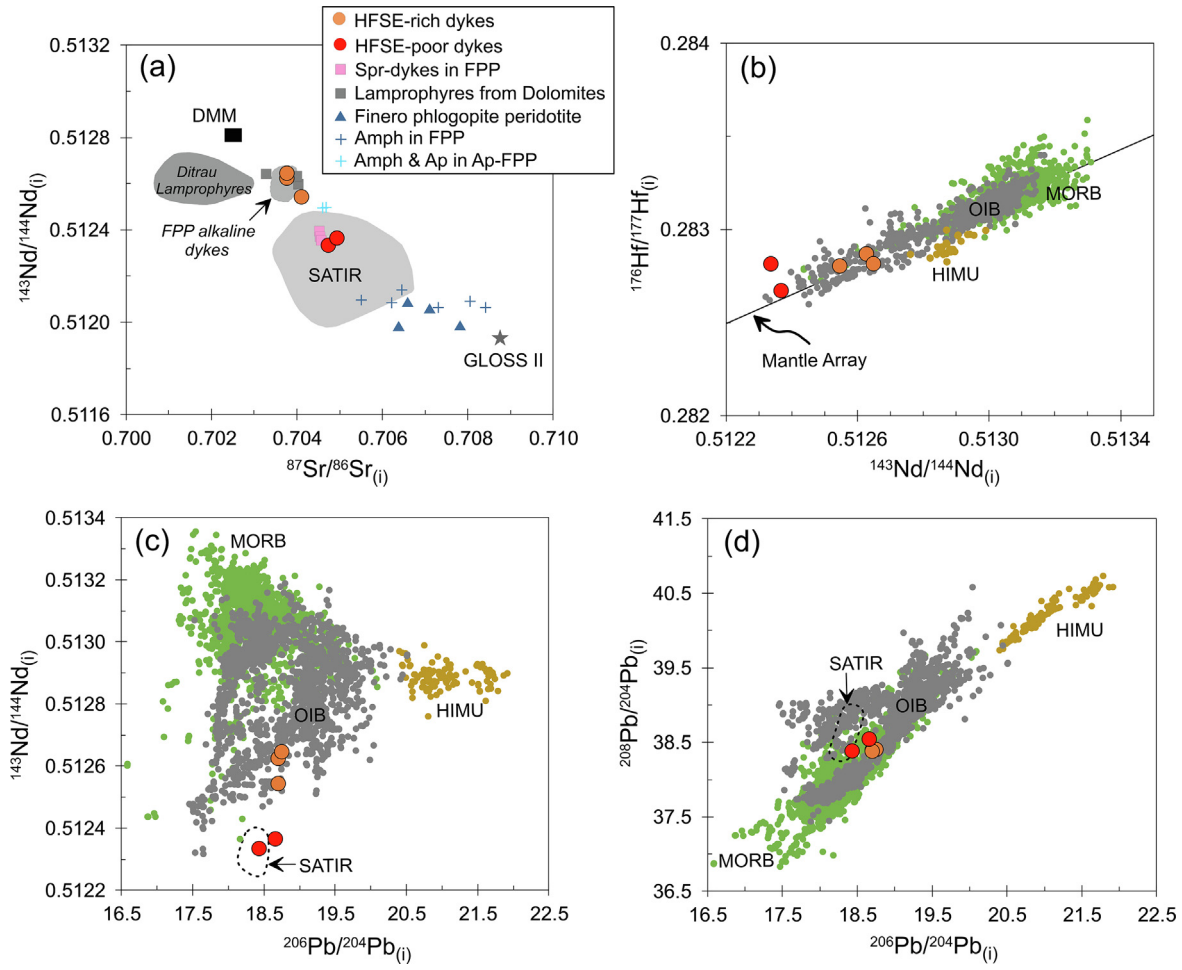

Fig. 11. Diagrams of (a) $^{87}Sr/^{86}Sr$ vs. $^{143}Nd/^{144}Nd$ (b) $^{143}Nd/^{144}Nd$ vs. $^{176}Hf/^{177}Hf$ (c) $^{206}Pb/^{204}Pb$ vs $^{143}Nd/^{144}Nd$ and (d) $^{206}Pb/^{204}Pb$ vs $^{208}Pb/^{204}Pb$ for amphiboles from the Finero HFSE-rich and HFSE-poor dyke samples (corrected to 200 Ma) compared to the Finero phlogopite peridotite (FPP, whole-rock, 295 Ma; Voshage et al., 1987), metasomatic amphiboles in the FPP (295 Ma; Obermiller, 1994; Giovanardi et al., 2020), amphibole and apatite from apatite-bearing layers in the FPP (215 Ma; Morishita et al., 2008), alkaline dykes in the FPP (225 Ma; Stähle et al., 2001), sapphirine-bearing gabbroic dykes in FPP (225 Ma; Giovanardi et al., 2020), alkaline lamprophyres from Predazzo, Dolomites (219 Ma; Casetta et al., 2019), Southern Alps Mid-Triassic magmatic rocks (SATIR; 230 Ma; Lustrino et al., 2019; Casetta et al., 2021), Ditrau lamprophyres (220 Ma; Batki et al., 2014), modern MORB, OIB and HIMU (Stracke, 2012), DMM (Salters and Stracke, 2004; corrected to 200 Ma), GLOSS-II (average global subducting sediments II; Plank, 2014; corrected to 320 Ma).

differentiated, maybe exsolved, volatile-rich melts. This event may also be related to pervasive fluid circulation causing the replacement of the melanocratic segregates initially made of amphiboles by phlogopite.

(iv) Occurrence of olivine-dominated peridotite and clinopyroxenite layers, inclusions and pods in the dykes, probably representing cumulates fractionated during early stages of melt percolation and crystallization.

(v) Chloritization of phlogopite and occurrence of allanite (especially in anorthosites) documenting late-stage fluid circulation.

The symmetric layering of the HFSE-poor gabbro and hornblendite dykes also suggests that their emplacement was due to several events of melt percolation and deformation along shear zones. Several amphibole crystals in the gabbro are cut by leucocratic layers of plagioclase evidencing that a forceful magma injection led to the enlargement of the conduits, as previously highlighted by Giovanardi et al., (2013, 2020). The composite dykes containing amphiboles with both HFSE-poor and -rich compositions undoubtedly confirm that the dykes' conduits were percolated by multiple melts with different geochemical compositions and affinities. The observed geochemical gradient in amphibole (HFSE and REE) from the core to margins of the composite diorite (FI2106) clearly indicates that an older HFSE-poor rock was percolated and overprinted by HFSE-rich melt(s) which produced HFSE-rich amphiboles.

In summary, the formation of the Finero dykes involved several melts with different compositions episodically percolating conduits within the FPP over a prolonged period. Injected mafic mantle melts, in the early stages of crystallization, probably segregated cumulus peridotites and clinopyroxenites, some of which are preserved as relics in the dykes' conduits. These mafic mantle melts after the fractionation of olivine, clinopyroxene and probably spinel became more evolved and segregated amphiboles and other phases present in the dykes. The amphibole + phlogopite + apatite ± plagioclase-dominated mineralogy of all the dykes coupled with the occurrence of primary calcite in them supports the assertion that they were derived from evolved mantle melts rich in volatiles (e.g. H_2O, P, CO_2, S, Cl, F).

6.2. Geochemical signatures and nature of parental melts

Major, trace and Nd-Sr isotopic compositions of amphiboles point to two distinct geochemical affinities of the melts that segregated the Finero dykes. The low HFSE content (Nb = 3.2–8.7 ppm; Ta = 0.1–0.3 ppm) coupled to the enrichment of LILE relative to HFSE (e.g. high Ba/Nb = 8–22) and suprachondritic Ti/Nb and

Zr/Nb ratios of amphibole from the HFSE-poor dykes indicates amphibole segregation from calc-alkaline melts with orogenic-like affinity (Coltorti et al., 2007). Amphibole from the HFSE-rich dykes, on the other hand, is characterized by high HFSE contents (Nb = 70–270 ppm; Ta = 1–12 ppm), enrichment in HFSE relative to LILE (e.g. low Ba/Nb commonly < 0.7), and chondritic to sub-chondritic Ti/Nb and Zr/Nb ratios, pointing to an alkaline to ultra-alkaline affinity of the parental melts. This assertion is further supported by (i) the occurrence of Nb-Ta-rich phlogopite, Nb-Ta oxides (e.g. columbite) and accessory titanite and ilmenite in the HFSE-rich dykes; and (ii) the common association of ultra-alkaline (-carbonatitic) magmatism, Nb-Ta deposits and albite-dominated anorthosites (or albitite) that is well-documented in literature (e.g., Pin et al., 2006; Galli et al., 2019).

The Nd and Sr isotopic compositions of the HFSE-rich and HFSE-poor dykes are also very different, supporting different melts affinities and sources (Fig. 11a). Amphibole from the HFSE-poor dykes is characterized by high radiogenic $^{87}Sr/^{86}Sr_{(200)}$ (0.704732 to 0.704934) and low radiogenic Nd isotopes ($\varepsilon Nd_{(200)}$ from –0.1 to –0.7). These values are very similar to those reported for the sapphirine-bearing gabbroic dykes from FPP (Giovanardi et al., 2020) and the Middle Triassic high-K calc-alkaline to shoshonitic lavas from Dolomites (Lustrino et al., 2019; Casetta et al., 2021; Nardini et al., 2022). This signature may be interpreted as the result of the interaction of ascending mantle melts with continental crust. Alternatively, it may be derived from ancient mantle sources that have experienced variable degrees of melt extractions and/or modifications in the form of digestion of subducted and/or delaminated material (e.g., Lustrino et al., 2011; Lustrino and Anderson, 2015; Lustrino et al., 2019; Giovanardi et al., 2020). The FPP and its constituent amphibole exhibits more radiogenic $^{87}Sr/^{86}Sr_{(i)}$ and unradiogenic $^{143}Nd/^{144}Nd_{(i)}$ (Giovanardi et al., 2020; Zanetti et al., 1999; Obermiller, 1994; Fig. 11a) indicating that the FPP had a larger fraction of crustal components than the melts that segregated the HFSE-poor dykes. However, the melts which formed the apatite-bearing layers within the FPP (Morishita et al., 2008; Fig. 11a) may be similar to the melts that segregated the HFSE-poor dykes. The Nd-Sr isotopic composition and high Al_2O_3, TiO_2 and K_2O contents of the HFSE-poor dykes, combined with those of the sapphirine-bearing gabbroic dykes and FPP, points to mantle sources containing significant amounts of continental crustal components. The radiogenic Pb isotopic composition of amphiboles from the HFSE-poor dykes ($^{206}Pb/^{204}Pb$ = 18.4–18.6; $^{207}Pb/^{204}Pb$ = 15.6; $^{208}Pb/^{204}Pb$ = 38.4–38.5) overlaps the field of OIB recording EMII-like characteristics of the mantle source, attesting to the involvement of significant amounts of recycled continental crust Pb components in the mantle source(s) of their parental melts. In the Nd-Pb diagram, the HFSE-poor dykes lie within the peculiar field defined by Southern Alps Middle Triassic Rocks (SATIR; Fig. 11c). The plot of the HFSE-poor dykes at the end of the OIB field on the Nd-Hf mantle array (Fig. 11b) and oxygen isotopic composition of amphibole and plagioclase from the sapphirine-bearing gabbroic dykes ($\delta^{18}O$ Amph = 6.86–6.94 ‰ SMOW; $\delta^{18}O$ Plag = 8.6 ‰ SMOW; Giovanardi et al., 2020) heavier than mantle composition (e.g., $\delta^{18}O$ of mantle peridotite, pyroxenite, and MORB = 5.7 ± 0.2 ‰ SMOW; Bindeman, 2008) are further evidence for the presence of substantial amounts of recycled continental crust components in the mantle sources and melts of the orogenic-like, HFSE-poor magmatism of Finero.

In contrast, amphibole from the HFSE-rich dykes exhibits relatively low radiogenic $^{87}Sr/^{86}Sr_{(200)}$ (0.703761–0.704103) and relatively high radiogenic Nd isotopes ($\varepsilon Nd_{(200)}$ from +3.4 to +5.4) plotting close to the DMM end-member and closely similar to the compositions of nepheline-bearing alkaline dykes from FPP and the alkaline lamprophyres from Predazzo, Dolomites (Stähle et al., 2001; Casetta et al., 2019). This signature is consistent with derivation from a more depleted mantle source. The Pb isotope data of amphiboles from the HFSE-rich dykes ($^{206}Pb/^{204}Pb$ = 18.7; $^{207}Pb/^{204}Pb$ = 15.6; $^{208}Pb/^{204}Pb$ = 38.4) are similar to those of the HFSE-poor dykes. This suggests that the mantle sources of both dyke groups contained recycled continental crustal components. However, the HFSE-rich dykes most probably incorporated less crustal components as indicated by its more depleted Nd, Sr and Hf isotopic compositions. It is also important to highlight here that we find no evidence of HIMU components in any of the investigated dykes from Finero, as suggested by Stälhe et al. (2001).

Equilibrium melts composition calculated from the trace element contents of amphiboles from representative samples of HFSE-poor and HFSE-rich dykes using experimentally determined amphibole-melt partition coefficients (dataset 47S; Tiepolo, 1999) are shown in Fig. 12 and are compared to the bulk-rock composition of Middle Triassic lavas and Late Triassic alkaline lamprophyres from the Dolomites. The incompatible trace element fractionation of the calculated HFSE-poor melt mimics that of the Middle Triassic high-K calc-alkaline to shoshonitic lavas from the Dolomites (Casetta et al., 2021). The major difference between our calculated HFSE-poor melt and the Dolomites shoshonites relates to absolute abundances particularly in Th, U, Nb, Ta and Pb which are higher in the calculated HFSE-poor melt. Notwithstanding, Nb-Ta in the HFSE-poor melt are less than the concentration in the alkaline lamprophyre from Predazzo, Dolomites (Casetta et al., 2019). The Predazzo alkaline lamprophyres however have significantly lower trace element content including Nb-Ta compared to the calculated HFSE-rich melt which appears ultra-alkaline and highly enriched in Nb, Ta, Zr and Hf (Fig. 12).

According to Coltorti et al. (2007), the geochemical features of calc-alkaline and intraplate magmatism can be reconciled by HFSE-depleted fluids coming off subducted crustal slab(s), leaving a rutile-bearing eclogite residuum rich in HFSE (mainly Nb, Ta and Ti). As the subduction process continues, the rutile-bearing eclogite further descends into the lower part of the upper mantle (or even below), generating a subchondritic Ti/Nb or Zr/Nb reservoir. Decarlis et al. (2023) suggested that crustal delamination processes may have occurred in the IVZ during the collapse of the Variscan chain far to the North, as testified by widespread metasomatism of the FPP. Following both hypotheses, the partial incorporation of crustal materials to different mantle domains via subduction and/or delamination may explain the genesis of the Finero HFSE-poor and HFSE-rich dykes and the crustal components might be

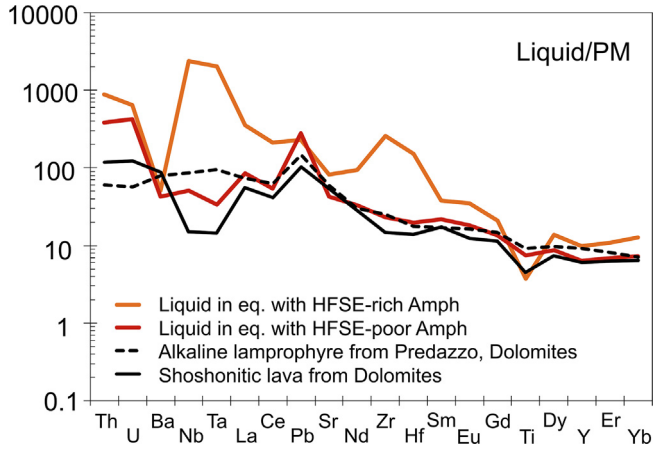

Fig. 12. Incompatible trace element patterns of melts calculated in equilibrium with amphiboles from representative samples of Finero HFSE-rich and HFSE-poor dykes. The bulk-rock composition of Late Triassic alkaline lamprophyre (Casetta et al., 2019) and Mid-Triassic shoshonitic lava (Casetta et al., 2021) from the Dolomites are also plotted for comparison. PM values are from McDonough and Sun (1995).

related to the Variscan and/or older orogenic cycles which were later triggered or remobilized until the Early Mesozoic. The presence of primary calcite in all the dykes supports the derivation of their parental melts from mantle sources probably containing some carbonatitic components. The possibility of assimilation of crustal rocks by the mantle-derived melts which segregated the Finero dykes is severely limited as they were very likely emplaced into the host mantle peridotite (FPP) when it was still at mantle levels (Zanetti et al., 2016; Decarlis et al., 2023). The idea of the FPP still at mantle levels under P $\geq$ 1.1 GPa until Mesozoic times is attested to by (i) the occurrence of sapphirine in our HFSE-poor gabbro sample and those investigated by Giovanardi et al., (2013, 2020), and (ii) amphibole-plagioclase thermometric calculation (Holland and Blundy, 1994) providing P-T conditions of dykes' emplacement at $\sim$ 660–1000 °C and $\sim$ 1 GPa. The geochemical signatures of the dykes are therefore primary features inherited from their mantle sources. The crustal imprints in mantle melts recorded by the studied dykes and the metasomatizing agents of the FPP could consequently imply that the subcontinental mantle sources beneath the Finero Complex and the IVZ at large continuously retained enriched subduction-related (Zanetti et al., 1999; Selverstone and Sharp, 2011; Cannaò et al., 2022) and/or delaminated crustal components (Decarlis et al., 2023) over a prolonged period of time. This contradicts an earlier conclusion by Casetta et al., (2019, 2021) that the generation of the Middle Triassic high-K calc-alkaline to shoshonitic magmas represents the exhaustion of the subduction-related signature in the Southern Alps lithosphere.

Based on petrographic, geochemical and isotopic data, and petrological reasoning, we recognize that the HFSE-poor magmatism occurred shortly before the HFSE-rich magmatism in Finero and IVZ. Therefore, there is no possibility of HFSE-poor magmas directly fractionating to HFSE-rich melts. We also exclude the possibility of the HFSE-poor dykes being products of residual melts after fractional crystallization and segregation of the HFSE-rich dykes. These hypotheses are premised on (i) the trace elements gradients observed in amphiboles and apatites from the composite dykes lending credence to the overprinting of older HFSE-poor amphiboles by HFSE-rich melts; (ii) close similarity of the geochemical and isotopic signatures of the HFSE-poor dykes with the Middle Triassic calc-alkaline to shoshonitic magmatism of Dolomites; (iii) similarity of the age, and geochemical and isotopic signatures of the HFSE-rich dykes with the Late Triassic alkaline lamprophyres of Dolomites and nepheline-bearing alkaline dykes from FPP; and (iv) the well-established temporal sequence of subduction, calc-alkaline volcanism and intraplate magmatism that has been documented in the Dolomites and several localities around the Mediterranean areas and in most subduction zones worldwide (Coltorti et al., 2007; Agostini et al., 2007; Zheng, 2019; Deng et al., 2023).

Hence, as a whole, the Finero dyke swarms record a geochemical change from orogenic-like magmatism, typical of post-collisional settings, to anorogenic alkaline magmatism, common in intraplate to extensional settings, pointing to a progressive variation of the mantle sources of the Southern Alps magmatism in response to the change of geodynamic environment during Early Mesozoic times.

6.3. Origin of cumulates in dykes

As earlier highlighted in section 6.1, olivine-dominated peridotite and clinopyroxenite layers, inclusions and pods occurring in the Finero dykes (e.g., Fig. 2a) are probably relics of cumulates segregated in the early stages of crystallization from the mantle-derived melts which evolved to produce the amphibole-dominated dykes. It is very likely that both HFSE-poor and HFSE-rich mantle-derived melts which percolated the FPP conduits crystallized and fractionated at least olivine at the beginning of crystallization leading to melts' evolution and subsequent crystallization of amphiboles and other mineral phases. Therefore, the composition of these cumulates and their relation to subsequent HFSE-poor and HFSE-rich amphiboles derived from more evolved melts is crucial to decipher the processes controlling the early stages of the magmatisms.

Olivine-dominated peridotite pods and inclusions occur in all the dyke groups and show similar composition, with forsterite (77–82), NiO (commonly < 0.32 wt%) and FeO_t (17–21 wt%) contents of olivine significantly outside the array of primary mantle peridotites (e.g., FPP olivine Fo = 90–92; NiO = 0.25–0.47 wt%; FeO_t=$\sim$9 wt%; Zanetti et al., 1999; Giovanardi et al., 2020). Low-forsterite olivine can be regarded as a product of (i) melt-rock interaction or (ii) crystallization from Fe-enriched evolved mantle melts. Melt-rock interaction can modify the composition of primary mantle peridotites; however, the forsterite content of the constituent mantle olivine can only be significantly decreased after interaction with very large amount of highly-evolved melts (Berno et al., 2020). A typical example is the FPP, which retains a highly depleted olivine composition (olivine Fo = 90–92) after multiple episodes of metasomatic modifications. On the other hand, during crystallization from primitive mantle-derived magmas containing > 6 wt% MgO, spinel (Cr-spinel and chromite) and high forsterite olivine are often the first phases to crystallize (Roeder et al., 2001, 2006). When these high-Mg# and Cr# phases separate, the residual melt evolves toward a Fe-enriched composition which can crystallize low-forsterite olivine. The olivine composition of the peridotites within the studied dykes can therefore result from crystallization from evolved Fe-enriched melts after the fractional crystallization and separation of high forsterite olivine and spinel. The absence of spinel in the olivine-dominated peridotites probably attests to their earlier fractionation out of the melts. Additionally, the low Ni/Co (<20) and Ni/Mn (<2) values of the olivines are typical of magmatic olivines (Wang et al., 2021).

Fe/Mn and Zn/Fe ratios in olivine are good proxies to decipher the signature of the mantle source region (peridotite or pyroxenite source) because the Fe/Mn ratio is largely unchanged by olivine fractionation (e.g., Søager et al., 2015) and Zn/Fe ratio appears to be temperature-independent within error (e.g., Le Roux et al., 2010). The Fe/Mn ($\sim$60–70) and Zn^*10^4/Fe (9–11) ratio of olivines from our cumulate peridotite pods exhibit values typical of magmas derived from the partial melting of primary mantle peridotites. The abundance of pyrite and pentlandite associated with the olivines reflects the metal (e.g., Fe and Ni) enrichment of the mantle melts and suggests derivation from a metal-rich source region. The occurrence of the olivine-dominated peridotite as pods and thin layers within the dykes also indicates that they are preserved relics after multiple percolations and interaction with subsequent HFSE-poor and HFSE-rich mantle melts. The formation of fine-grained interstitial orthopyroxene between olivines and amphiboles indicates interaction between the olivine-dominated peridotite and subsequent melts. We therefore, tentatively suggest that the olivine-dominated peridotite pods/layers are related to their host dykes, whether HFSE-poor or -rich, by fractionation process.

Clinopyroxenite cumulates are only associated with the HFSE-rich dykes (in diorites and hornblendites) probably documenting an additional mineral phase (clinopyroxene) fractionated after olivine from HFSE-rich melts in the FPP conduits. Clinopyroxenes from the clinopyroxenite cumulates exhibit similar REE contents and chondrite-normalized patterns with the amphiboles from the HFSE-rich dykes. This suggests an equilibrium between the clinopyroxenes and amphiboles pointing to cognate alkaline melt sources. On this basis, the clinopyroxenites are inferred to be seg-

regates fractionated from HFSE-rich melts pulses intruded into FPP during Early Mesozoic times.

6.4. Is the Finero Phlogopite Peridotite a possible mantle source of the Early Mesozoic magmatism in the Southern Alps?

Conceição and Green (2004) have demonstrated via high-pressure and -temperature melting experiments that primary shoshonitic magmas may be produced by decompression melting of phlogopite- and pargasite-bearing peridotites at ~ 1 GPa and 1050–1150 °C. On the other hand, alkaline, volatile-rich magmas segregating amphibole-rich rocks have also been modelled to originate by low-degree partial melting of similar mantle domains, but at higher pressures (≥3 GPa), possibly at the asthenosphere–litho sphere boundary (Foley, 1990; Tappe et al., 2006). In light of these experimental constraints coupled with the Nb-Ta-Ti-depleted composition and mineralogical make-up of the FPP by metasomatic amphibole, phlogopite, and sometimes apatite and carbonates, an assumption of the generation of the melts segregating the studied HFSE-poor dykes from a similar metasomatized lithospheric mantle is reasonable. The modeling of the source composition of the Middle Triassic shoshonitic magmatism of Dolomites by Casetta et al. (2021) suggests that the Finero Phlogopite Peridotite is the best approximation of the mantle source of the HFSE-poor, shoshonitic magmatism during this time. The HFSE-rich alkaline melts may also be generated from a Finero-like mantle but with enrichments in Nb-Ta from a deeply subducted/recycled rutile-bearing eclogitic slab at asthenospheric to deep lithospheric depths. The depleted Nd, Sr and Hf isotopic compositions of the HFSE-rich dykes suggests that they were predominantly derived from an asthenospheric mantle source; however, the contribution of a deep lithospheric mantle source to their parental melts cannot be excluded. Possible mechanisms of formation of the HFSE-rich alkaline melts may include: (i) partial melting of an upwelling depleted asthenosphere interacting with enriched/metasomatized deep lithospheric mantle components (e.g., Casetta et al., 2019); (ii) partial melting of an upwelling depleted asthenosphere interacting with small volumes of enriched melts derived from melting of deeply subducted rutile-bearing eclogitic slab; and/or (iii) partial melting of enriched asthenosphere. A good approximation of the mantle source lithology could be a garnet peridotite with or without phlogopite, K-richterite and calcite (e.g., Tappe et al., 2006).

6.5. Geodynamic perspective

The Early Mesozoic orogenic-like magmatism of the Ivrea-Verbano Zone originated by decompression partial melting of metasomatized lithospheric mantle sources at relatively lower pressures. The subsequent alkaline anorogenic magmatism was possibly derived by low-degree partial melting of asthenospheric to deep lithospheric mantle sources. This transition clearly indicates that the mantle source regions in the IVZ changed through times. The heterogeneity of the mantle beneath the eastern (e.g., Dolomites) and central (e.g., Brescian Prealps) sectors of the Southern Alps has also been documented by a change in the geochemical signatures of the Early Mesozoic magmatism from high-K calc-alkaline to shoshonitic affinity during the Middle Triassic to alkaline affinity during the Late Triassic (Cassinis et al., 2008; De Min et al., 2020; Casetta et al., 2019, 2021). This correlation and similarity in geochemical signatures strongly indicate that similar tectonic and magmatic processes/events occurred throughout the Southern Alps after the Variscan orogeny s.s.

Variscan orogeny in the European area resulted from a complex setting which details is still a matter of debate. The principal components of this tectonic scenario were Gondwana s.l. (to the South) and Laurussia continental plates (to the North). Their collision in the Carboniferous resulted in the formation of the Hercinian-Variscan Cordillera, following the closure of the Rhenohercinian Ocean (e.g. Stampfli and Borel, 2004 and references therein). The Hercinian-Variscan belt was connected to the Appalachian region to the west by a complex range, probably dominated by wrench tectonics. Following one of the most popular paleogeographic interpretation of the Alpine region (e.g. Stampfli and Kozur, 2006), the Variscan collision in the present-day Western European area occurred between Laurussia and the Hunic/Galatian superterrane (Stampfli et al., 2002; von Raumer et al., 2013), a sector of Gondwana that drifted away from the main continent after the onset of the Paleotethys ocean during the Silurian (Stampfli and Borel, 2004; von Raumer et al., 2013). Adria microplate was located at the southern termination of this superterrane, and rested in the outskirts of the Variscan Cordillera s.s. during Late Carboniferous collision (Fig. 13a-b).

Thus, the Southern Alps (and the IVZ at depths) were located between the Variscan collisional system to the North and a mature Paleotethys oceanic system to the South. During the Late Carboniferous, the overthickened Variscan crust started to collapse in a post-collisional environment (Fig. 13b-c; Burg et al., 1994). Following the interpretation of Decarlis et al. (2023), the delamination of the lower crust led to the detachment of wide slabs from the root of the chain that sunk into the mantle favouring mixing of the mantle with continental melts, as possibly documented by the ca. 315–310 Ma pervasive metasomatism of the FPP mantle section (Fig. 13b-c). This event was concomitant to the widespread eruption of K-rich lamprophyres throughout the Variscan realm in the 340–280 Ma time interval following the Variscan orogeny peak (Soder and Romer, 2018). The presence of continental crust component is also documented in primary mantle magmas intruded into the Southern Variscides (Southern Alps and Corsica) in the Lower Permian post-collisional magmatic climax (290–280 Ma; Boscaini et al., 2020).

Later on, following the interpretation of Casetta et al. (2021), the influence of the Paleotethys active margin became more and more relevant in the Alpine region and eventually, in the Triassic, the Paleotethys subduction system triggered the magmatism of the Southern Alps. This setting, still ascribed by several authors to the "Variscan cycle", may be regarded as the paleotectonic scenario in which the Early Mesozoic Finero dykes with orogenic-like affinity, object of the present study, may have developed (Fig. 13d).

It is very difficult and beyond the scope of this paper, to assess the exact paleogeographic context of the region. Several solutions were proposed to explain the continuous extension in the Southalpine domain during the Triassic and the relationships with the subduction of Paleotethys and/or later oceanic troughs (e.g. Channell and Kozur, 1997; Stampfli and Borel, 2004; Handy et al., 2010; van Hinsbergen et al., 2020). The solution in Fig. 13c-d may represent a mere oversimplification of the real system (taken from Casetta et al., 2021; Stampfli and Borel, 2004; modified). However, this interpretation is at the moment purely speculative and requires further investigation. The relatively long distance of the Southalpine domain from the subduction area may represent a limitation and open the possibility that other factors may have contributed to the continental contamination of the Finero mantle section (e.g. late melting or reaction of remnant of slabs of the Variscan belt present in the mantle). Especially, the major challenge is represented by the peculiar position occupied by the Adriatic plate during the Variscan and early Alpine cycles, which since Late Carboniferous onward, remained at the North-westernmost termination of the Paleotethys. The area was at first characterized by a wrenching connection with the westernmost sectors (Fig. 13b-c), then possibly acted as a "pivot" for the Cimmerian Terranes (Fig. 13c-d) and finally underwent extreme extension leading to

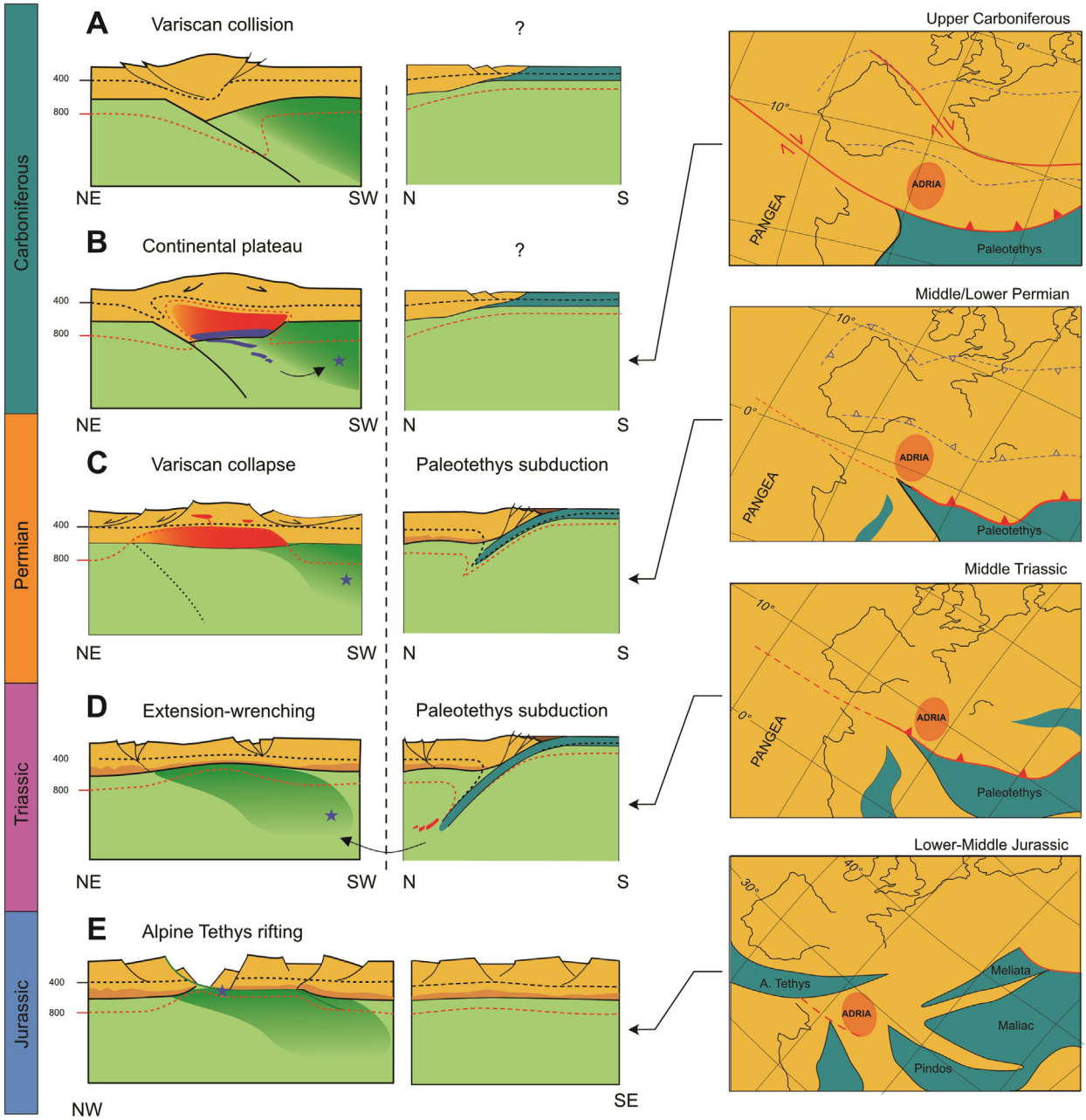

Fig. 13. Schematic diagrams of the possible evolution of the Southalpine domain during the Late Paleozoic-Early Mesozoic interval derived from literature and personal observations in the Ivrea-Verbano Zone (blue star: suggested position of the Finero massif). (a, b) Late Variscan cycle, progressive thickening of the continental crust leading to delamination and contamination of the Finero peridotite (from Decarlis et al., 2023; Casetta et al., 2021; Stampfli and Kozur, 2006); (c) Collapse of the Variscan belt to the west accompanied by subduction of the Paleotethys oceanic domain in the southernmost sector (Casetta et al., 2021); (d) Diffused extensional tectonics in the western-central Southalpine sector and protracted Paleotethys subduction to the south; triggering of Southalpine magmatism and possible mantle crustal contamination (Casetta et al., 2021); (e) Initiation of Alpine Tethys rifting and formation of the distal margin in the Western Southalpine domain (e.g. Beltrando et al., 2015; Decarlis et al., 2017 and references therein). To the southeast, the system passes to a complex tectonic scenario, still matter of debate, in which different extensional basins may have existed (e.g. Channell and Kozur, 1997), here oversimplified with a generalized extension. See text for detailed descriptions. Paleogeographic plate reconstructions from Borel and Stampfli, 2004; Stampfli and Kozur, 2006; modified.

the opening of the Alpine Tethys (Fig. 13e; Decarlis et al., 2017; Beltrando et al., 2015). It was in this latter context that the studied anorogenic dykes were probably emplaced. In fact, starting from the late Triassic onwards (Beltrando et al., 2015), the thermal structure of the Adriatic lithosphere underwent a profound reorganization. Changes started early at mantle depths, as testified by the evidence of the Finero magmatism, and later became evident in the upper crust as a progressive increase of stretching that culminated with hyperextension and exhumation of the mantle to the surface (e.g. Decarlis et al., 2015, 2017; Petri et al., 2023). This dynamics was tentatively simulated using numerical modelling by Chenin et al. (2019).

On a final note, both the orogenic-like and alkaline anorogenic magmatisms in the IVZ and those in the central and eastern sectors of the Southern Alps occurred during a period of protracted extension in the Early Mesozoic that started at ca. 245 Ma and continued up to ca. 170–160 Ma culminating with the Alpine Tethys emplacement (Schettino and Turco, 2011; Denyszyn et al., 2018).

However, notwithstanding the occurrence of the orogenic-like magmatism of the Southern Alps in transtensional to extensional settings, its geochemical signature is typical of post-collisional tectonic settings (Stampfli and Borel, 2002, 2004; Doglioni, 2007; Zanetti et al., 2013; Casetta et al., 2018; De Min et al., 2020). On the other hand, the successive alkaline to ultra-alkaline magmatism are more frankly related to a rift-related asthenospheric upwelling event in an intraplate geodynamic setting, and probably represent a precursor of the rifting stage connected to the Alpine Tethys opening in the western Mediterranean region (Stälhe et al., 2001; Mazzucchelli et al., 2010; Schaltegger et al., 2015; Galli et al., 2019; Casetta et al., 2019; Bonazzi et al., 2020; Giovanardi et al., 2020; De Min et al., 2020).

7. Concluding remarks

Detailed geochemical and isotopic characterization of Early Mesozoic dyke swarms cross-cutting the Finero phlogopite peridotite in the Ivrea-Verbano Zone identified three varieties on the basis of their HFSE enrichments: HFSE-poor, HFSE-rich and composite HFSE-poor and -rich dykes. These dykes record a geochemical change from orogenic-like calc-alkaline magmatism derived from metasomatized lithospheric mantle sources at relatively lower pressures, to alkaline anorogenic magmatism possibly derived from low-degree partial melting of asthenospheric to deep lithospheric mantle sources indicating a progressive variation of the mantle sources of the Southern Alps magmatism during Early Mesozoic times. These Early Mesozoic magmatisms also provide evidence that the mantle sources beneath the Southern Alps continuously retained subduction-related and/or delaminated crustal components over a prolonged period of time probably from the Variscan and/or older times up to the Triassic–Jurassic boundary. The transition of the geochemical affinities of the Early Mesozoic magmatism in the IVZ in combination with geochemical records from the Dolomites and the Brescian Prealps further attests to the complex and diverse magmatic events that characterizes the Southern Alps in response to changing geodynamic regimes after the Variscan orogeny and shortly before the break-up and dispersal of the Pangea.

CRediT authorship contribution statement

Abimbola C. Ogunyele: Data curation, Formal analysis, Investigation, Methodology, Validation, Visualization, Writing – original draft, Writing – review & editing. **Mattia Bonazzi:** Formal analysis, Investigation, Methodology, Writing – review & editing. **Tommaso Giovanardi:** Data curation, Formal analysis, Investigation, Methodology, Validation, Visualization, Writing – review & editing. **Maurizio Mazzucchelli:** Conceptualization, Funding acquisition, Investigation, Supervision, Writing – review & editing. **Vincent J. M. Salters:** Funding acquisition, Investigation, Supervision, Writing – review & editing. **Alessandro Decarlis:** Funding acquisition, Writing – review & editing. **Alessio Sanfilippo:** Supervision, Writing – review & editing. **Alberto Zanetti:** Conceptualization, Funding acquisition, Methodology, Project administration, Resources, Supervision, Validation, Visualization, Writing – review & editing.

Declaration of competing interest

The authors declare that they have no known competing financial interests or personal relationships that could have appeared to influence the work reported in this paper.

Acknowledgements

ACO acknowledges the support of the University of Pavia, Italy for a doctoral scholarship and an international mobility grant to visit the National High Magnetic Field Laboratory, Florida State University, USA to conduct some analytical work reported in this manuscript. VJMS was supported by National Science Foundation (NSF, USA) grant OCE 2126496. Part of this work was performed at the National High Magnetic Field Laboratory, which is supported by National Science Foundation Cooperative Agreement No. DMR-1157490 and the State of Florida. A.Z. was supported by the Italian "Programma di Rilevante Interesse Nazionale" project PRIN_20178LPCPW. MM and TG were supported by FAR 2023 project of the Università di Modena e Reggio Emilia, Italy. The Handling Editor, Taras Gerya, and two anonymous reviewers are thanked for their constructive reviews.

Appendix A. Supplementary material

Supplementary data to this article can be found online at https://doi.org/10.1016/j.gr.2023.12.011.

References

Agostini, S., Doglioni, C., Innocenti, F., Manetti, P., Tonarini, S., and Savasçin, M.Y., 2007. The transition from subduction-related to intraplate Neogene magmatism in the Western Anatolia and Aegean area, *in* Beccaluva, L., Bianchini, G., and Wilson, M., eds., Cenozoic Volcanism in the Mediterranean Area. Geol. Soc. Am. Spec. Paper 418, 1–15. https://doi.org/10.1130/2007.2418(01).

Batki, A., Pal-Molnar, E., Dobosi, G., Skelton, A., 2014. Petrogenetic significance of ocellar camptonite dykes in the Ditrau Alkaline Massif, Romania. Lithos 200, 181–196. https://doi.org/10.1016/j.lithos.2014.04.022.

Beltrando, M., Stockli, D.F., Decarlis, A., Manatschal, G., 2015. A crustal-scale view at rift localization along the fossil Adriatic margin of the Alpine Tethys preserved in NW Italy. Tectonics 34. https://doi.org/10.1002/2015TC003973.

Berno, D., Tribuzio, R., Zanetti, A., Hémond., C., 2020. Evolution of mantle melts intruding the lowermost continental crust: constraints from the Monte Capio–Alpe Cevia mafic–ultramafic sequences (Ivrea–Verbano Zone, northern Italy). Contrib. Miner. Petrol. 175. https://doi.org/10.1007/s00410-019-1637-8.

Bindeman, I., 2008. Oxygen isotopes in mantle and crustal magmas as revealed by single crystal analysis. Rev. Miner. Geochem. 69, 445–478. https://doi.org/10.2138/rmg.2008.69.12.

Bonazzi, M., Ogunyele, A.C., Giovanardi, T., Mazzucchelli, M., Zanetti, A., 2022. Geochemistry and U-Pb geochronology of zircons from diorite to anorthosite dykes intruding the Finero Phlogopite Peridotite (Ivrea-Verbano Zone): Evidence for a prolonged mantle-derived alkaline magmatism from the Upper Triassic to the Lower Jurassic in the Southern Alps. Earth Mantle Workshop (Abstract), Toulouse France, 11-15 Sept., 2022.

Bonazzi, M., Langone, A., Tumiati, S., Dellarole, E., Mazzucchelli, M., Giovanardi, T., Zanetti, A., 2020. Mantle-derived corundum-bearing felsic dykes may survive only within the lower (refractory/inert) crust: Evidence from zircon geochemistry and geochronology (Ivrea–Verbano Zone, Southern Alps, Italy). Geosci. 10, 281. https://doi.org/10.3390/geosciences10080281.

Boscaini, A., Marzoli, A., Davies, J.F.H.L., Chiaradia, M., Bertrand, H., Zanetti, A., Visonà, D., De Min, A., Jourdan, F., 2020. Permian post-collisional basic magmatism from Corsica to the Southeastern Alps. Lithos 376–377. https://doi.org/10.1016/j.lithos.2020.105733.

Burg, J.P., Van Den Driessche, J., Brun, J.P., 1994. Syn- to post-thickening extension in the Variscan Belt of Western Europe: modes and structural consequences. Géol. Fr. 3, 33–51.

Cannaò, E., Tiepolo, M., Fumagalli, P., Grieco, G., Agostini, S., 2022. Metasomatism in the Finero Phlogopite Peridotite: New insights from C and N concentrations and δ13C-δ11B signatures. Chem. Geol. 614. https://doi.org/10.1016/j.chemgeo.2022.121181.

Casetta, F., Coltorti, M., Marocchino, E., 2018. Petrological evolution of the Middle Triassic Predazzo Intrusive Complex, Italian Alps. Inter. Geol. Rev. 60, 977–997. https://doi.org/10.1080/00206814.2017.1363676.

Casetta, F., Ickert, R.B., Mark, D.F., Bonadiman, C., Giacomoni, P.P., Ntaflos, T., Coltorti, M., 2019. The alkaline lamprophyres of the Dolomitic Area (Southern Alps, Italy): markers of the late Triassic change from orogenic-like to anorogenic magmatism. J. Petrol. 60, 1263–1298. https://doi.org/10.1093/petrology/egz031.

Casetta, F., Ickert, R.B., Mark, D.F., Giacomoni, P.P., Bonadiman, C., Ntaflos, T., Zanetti, A., Coltorti, M., 2021. The Variscan subduction inheritance in the Southern Alps Sub-Continental Lithospheric Mantle: Clues from the Middle Triassic

shoshonitic magmatism of the Dolomites (NE Italy). Lithos, 380–381. https://doi.org/10.1016/j.lithos.2020.105856.
Cassinis, G., Cortesogno, L., Gaggero, L., Perotti, C.R., Buzzi, L., 2008. Permian to Triassic geodynamic and magmatic evolution of the Brescian Prealps (Eastern Lombardy, Italy). Ital. J. Geosci. 127, 501–518.
Channell, J.E.T., Kozur, H.W., 1997. How many oceans? Meliata, Vardar and Pindos oceans in Mesozoic Alpine paleogeography. Geology 25, 183–186. https://doi.org/10.1130/0091-7613(1997)025<0183:HMOMVA>2.3.CO;2.
Chenin, P., Manatschal, G., Decarlis, A., Schmalholz, S.M., Duretz, T., Beltrando, M., 2019. Emersion of distal domains in advanced stages of continental rifting explained by asynchronous crust and mantle necking. Geochem. Geophys. Geosys. 20, 3821–3840. https://doi.org/10.1029/2019GC008357.
Coltorti, M., Beccaluva, L., Bonadiman, C., Faccini, B., Ntaflos, T., Siena, F., 2004. Amphibole genesis via metasomatic reaction with clinopyroxene in mantle xenoliths from Victoria Land, Antarctica. Lithos 75, 115–139. https://doi.org/10.1016/j.lithos.2003.12.021.
Coltorti, M., Bonadiman, C., Faccini, B., Grégoire, M., O'Reilly, S.Y., Powell, W., 2007. Amphiboles from suprasubduction and intraplate lithospheric mantle. Lithos 99, 68–84. https://doi.org/10.1016/j.lithos.2007.05.009.
Conceição, R.V., Green, D.H., 2004. Derivation of potassic (shoshonitic) magmas by decompression melting of phlogopite+pargasite lherzolite. Lithos 72, 209–229. https://doi.org/10.1016/j.lithos.2003.09.003.
Corvò, S., Langone, A., Padrón-Navarta, J.A., Tommasi, A., Zanetti, A., 2020. Porphyroclasts: Source and sink of major and trace elements during deformation-induced metasomatism (Finero, Ivrea-Verbano Zone, Italy). Geosci. 10, 196. https://doi.org/10.3390/geosciences10050196.
De Min, A., Velicogna, M., Ziberna, L., Chiaradia, M., Alberti, A., Marzoli, A., 2020. Triassic magmatism in the European Southern Alps as an early phase of Pangea break-up. Geol. Mag. 157, 1–23. https://doi.org/10.1017/S0016756820000084.
Decarlis, A., Manatschal, G., Haupert, I., Masini, E., 2015. The tectono-stratigraphic evolution of distal, hyper-extended magma-poor conjugate rifted margins: Examples from the Alpine Tethys and Newfoundland-Iberia. Mar. Pet. Geol. 68, 54–72. https://doi.org/10.1016/j.marpetgeo.2015.08.005.
Decarlis, A., Beltrando, M., Manatschal, G., Ferrando, S., Carosi, R., 2017. Architecture of the distal Piedmont-Ligurian rifted margin in NW Italy: Hints for a flip of the rift system polarity. Tectonics 36. https://doi.org/10.1002/2017TC004561.
Decarlis, A., Zanetti, A., Ogunyele, A.C., Ceriani, A., Tribuzio, R., 2023. The Ivrea-Verbano tectonic evolution: The role of the crust-mantle interactions in rifting localization. Earth-Sci. Rev. 238. https://doi.org/10.1016/j.earscirev.2023.104318.
Deng, H., Kusky, T., Bozurt, E., Chen, C., Wang, L., Dong, Z., Meng, J., 2023. Sr-Nd-Ca isotopic variations of Cenozoic calc-alkaline and alkaline volcanic rocks above a slab tear in Western Anatolia, Turkey. GSA Bull. https://doi.org/10.1130/B36672.1.
Denyszyn, S.W., Fiorentini, M.L., Maas, R., Dering, G., 2018. A bigger tent for CAMP. Geology 46, 823–826. https://doi.org/10.1130/G45050.1.
Doglioni, C., 2007. Tectonics of the dolomites. Bull. Ang. Geol. 12, 11–15.
Foley, S., 1990. A review and assessment of experiments on kimberlites, lamproites and lamprophyres as a guide to their origin. Proc. Indian Acad. Sci. 99, 57–80. https://doi.org/10.1007/BF02871896.
Galli, A., Grassi, D., Sartori, G., Gianola, O., Burg, J.P., Schmidt, M.W., 2019. Jurassic carbonatite and alkaline magmatism in the Ivrea zone (European Alps) related to the breakup of Pangea. Geology 47, 199–202. https://doi.org/10.1130/G45678.1.
Giovanardi, T., Morishita, T., Zanetti, A., Mazzucchelli, M., Vannucci, R., 2013. Igneous sapphirine as a product of melt-peridotite interactions in the Finero Phlogopite Peridotite Massif, Western Italian Alps. Eur. J. Miner. 25, 17–31. https://doi.org/10.1127/0935-1221/2013/0025-2251.
Giovanardi, T., Zanetti, A., Dallai, L., Morishita, T., Hémond, C., Mazzucchelli, M., 2020. Evidence of subduction-related components in sapphirine-bearing gabbroic dykes (Finero phlogopite–peridotite): Insights into the source of the Triassic-Jurassic magmatism at the Europe-Africa boundary. Lithos 356–357,. https://doi.org/10.1016/j.lithos.2020.105366 105366.
Gregoire, M., McInnes, B.I.A., O'Reilly, S.Y., 2001. Hydrous metasomatism of oceanic sub-arc mantle, Lihir, Papua New Guinea–Part 2. Trace element characteristics of slab-derived fluids. Lithos 59, 91–108. https://doi.org/10.1016/S0024-4937(01)00058-5.
Grieco, G., Ferrario, A., von Quadt, A., Köppel, V., Mathez, A., 2001. The zircon-bearing chromitites of the phlogopite peridotite of Finero (Ivrea Zone, Southern Alps): evidence and geochronology of a metasomatized mantle slab. J. Petrol. 42, 89–101. https://doi.org/10.1093/petrology/42.1.89.
Griffin, W.L., Powell, W.J., Pearson, N.J., O'Reilly, S.Y., 2008. GLITTER: data reduction software for laser ablation ICPMS. In: Sylvester, P. (Ed.), Laser Ablation ICP–MS in the Earth Sciences: Current Practices and Outstanding Issues. Mineral. Assoc. Canada Short Course Series 40, pp. 308–311.
Handy, M., Franz, L., Heller, F., Janott, B., Zurbriggen, R., 1999. Multistage accretion, orogenic stacking, and exhumation of continental crust (Ivrea crustal section, Italy and Switzerland). Tectonics 18, 1154–1177.
Handy, M.R., Schmid, S.M., Bousquet, R., Kissling, E., Bernoulli, D., 2010. Reconciling plate-tectonic reconstructions of Alpine Tethys with the geological-geophysical record of spreading and subduction in the Alps. Earth-Sci. Rev. 102, 121–158. https://doi.org/10.1016/j.earscirev.2010.06.002.
Handy, M.R., Giese, J., Schmid, S.M., Pleuger, J., Spakman, W., Onuzi, K., Ustaszewski, K., 2019. Coupled crust-mantle response to slab tearing, bending, and rollback along the Dinaride-Hellenide orogen. Tectonics 38, 2803–2828. https://doi.org/10.1029/2019TC005524.
Harangi, S., Downes, H., Thirlwall, M., Gméling, K., 2007. Geochemistry, petrogenesis and geodynamic relationships of Miocene calc-alkaline volcanic rocks in the Western Carpathian Arc, Eastern Central Europe. J. Petrol. 48, 2261–2287. https://doi.org/10.1093/petrology/egm059.
Hawthorne, F.C., Oberti, R., Harlow, G.E., Maresch, W.V., Martin, R.F., Schumacher, J.C., Welch, M.D., 2012. Nomenclature of the amphibole supergroup. Am. Mineral. 97, 2031–2048. https://doi.org/10.2138/am.2012.4276.
Holland, T., Blundy, J., 1994. Non-ideal interactions in calcic amphiboles and their bearing on amphibole-plagioclase thermometry. Contr. Mineral. Petrol. 116, 433–447. https://doi.org/10.1007/BF00310910.
Ishimaru, S., Arai, S., Ishida, Y., Shirasaka, M., Okrugin, M., 2007. Melting and multi-stage metasomatism in the mantle wedge beneath a frontal arc inferred from highly depleted peridotite xenoliths from the Avacha volcano, southern Kamchatka. J. Petrol. 48, 1–39. https://doi.org/10.1093/petrology/egl065.
Kretz, R., 1983. Symbols for rock-forming minerals. Am. Mineral. 68, 277–279.
Langone, A., José, A.P.N., Ji, W.Q., Zanetti, A., Mazzucchelli, M., Tiepolo, M., Giovanardi, T., Bonazzi, M., 2017. Ductile–brittle deformation effects on crystal-chemistry and U-Pb ages of magmatic and metasomatic zircons from a dyke of the Finero Mafic Complex (Ivrea–Verbano Zone, Italian Alps). Lithos 284, 493–511. https://doi.org/10.1016/j.lithos.2017.04.020.
Langone, A., Zanetti, A., Daczko, N.R., Piazolo, S., Tiepolo, M., Mazzucchelli, M., 2018. Zircon U-Pb dating of a lower crustal shear zone: a case study from the northern sector of the Ivrea-Verbano Zone (Val Cannobina, Italy). Tectonics 37, 322–342.
Le Roux, V., Lee, C.-T.-A., Turner, S.J., 2010. Zn/Fe systematics in mafic and ultramafic systems: Implications for detecting major element heterogeneities in the Earth's mantle. Geochim. Cosmochim. Acta 74, 2779–2796. https://doi.org/10.1016/j.gca.2010.02.004.
Lustrino, M., Anderson, D.L., 2015. The mantle isotopic printer: basic mantle plume geochemistry for seismologists and geodynamicists. Geol. Soc. Am. Spec. Pap. 514, 257–279.
Lustrino, M., Duggen, S., Rosenberg, C.L., 2011. The Central-Western Mediterranean: anomalous igneous activity in an anomalous collisional tectonic setting. Earth-Sci. Rev. 104, 1–40. https://doi.org/10.1016/j.earscirev.2010.08.002.
Lustrino, M., Fedele, L., Melluso, L., Morra, V., Ronga, F., Geldmacher, J., Duggen, S., Agostini, S., Cucciniello, C., Franciosi, L., Meisel, T., 2013. Origin and evolution of Cenozoic magmatism of Sardinia (Italy). A combined isotopic (Sr–Nd–Pb–O–Hf–Os) and petrological view. Lithos 180–181, 138–158. https://doi.org/10.1016/j.lithos.2013.08.022.
Lustrino, M., Abbas, H., Agostini, S., Caggiati, M., Carminati, E., Gianolla, P., 2019. Origin of Triassic magmatism of the Southern Alps (Italy): Constraints from geochemistry and Sr-Nd-Pb isotopic ratios. Gondwana Res. 75, 218–238. https://doi.org/10.1016/j.gr.2019.04.011.
Lyubetskaya, T., Korenaga, J., 2007. Chemical composition of Earth's primitive mantle and its variance: 1. Method and results. J. Geophys. Res. Solid Earth 112, B03211. https://doi.org/10.1029/2005JB004223.
Marquez, A., Oyarzum, R., Doblas, M., Verma, S.P., 1999. Alkalic (ocean island basalt type) and calc-alkalic volcanism in Mexican volcanic belt: A case of plume-related magmatism and propagating rifting at an active margin? Geology 27, 51–54. https://doi.org/10.1130/0091-7613(1999)027<0051:AOIBTA>2.3.CO;2.
Mazzucchelli, M., Zanetti, A., Rivalenti, G., Vannucci, R., Correia, C.T., Tassinari, C.C.G., 2010. Age and geochemistry of mantle peridotites and diorite dykes from the Baldissero body: Insights into the Paleozoic-Mesozoic evolution of the Southern Alps. Lithos 119, 485–500. https://doi.org/10.1016/j.lithos.2010.08.002.
McDonough, W.F., Sun, S., 1995. The composition of the Earth. Chem. Geol. 120, 223–253. https://doi.org/10.1016/0009-2541(94)00140-4.
Moine, B.N., Gregoire, M., O'Reilly, S.Y., Sheppard, S.M.F., Cottin, J.-Y., 2001. High field strength element fractionation in the upper mantle: evidence from amphibole-rich composite mantle xenoliths from the Kerguelen Islands (Indian Ocean). J. Petrol. 42, 2145–2167. https://doi.org/10.1093/petrology/42.11.2145.
Morishita, T., Hattori, K.H., Terada, K., Matsumoto, T., Yamamoto, K., Takebe, M., Ishida, Y., Tamura, A., Arai, S., 2008. Geochemistry of apatite-rich layers in the Finero phlogopite–peridotite massif (Italian Western Alps) and ion microprobe dating of apatite. Chem. Geol. 251, 99–111. https://doi.org/10.1016/j.chemgeo.2008.02.018.
Nardini, N., Casetta, F., Ickert, R.B., Mark, D.F., Ntaflos, T., Zanetti, A., Coltorti, M., 2022. From the Middle Triassic Cima Pape complex (Dolomites; Southern Alps) to the feeding systems beneath active volcanoes: Clues from clinopyroxene textural and compositional zoning. J. Volcan. Geotherm. Res. 422. https://doi.org/10.1016/j.jvolgeores.2021.107459.
Obermiller, W.A., 1994. Chemical and Isotopic Variations in the Balmuccia, Baldissero and Finero Peridotite Massifs (Ivrea-Zone, N-Italy). Unpublished PhD thesis. Johannes-Gutenberg-Universität Mainz, p. 191.
Ogunyele, A.C., Giovanardi, T., Bonazzi, M., Mazzucchelli, M., Zanetti, A., 2021. Geochemistry and geochronology of alkaline dykes from the Finero Phlogopite Peridotite (Ivrea-Verbano Zone): insights into the Triassic-Jurassic tectono-magmatic events of the Southern Alps. EGU Gen. Ass. Abstract (EGU21-10286). https://doi.org/10.5194/egusphere-egu21-10286.
Peressini, G., Quick, J.E., Sinigoi, S., Hofmann, A.W., Fanning, M., 2007. Duration of a large mafic intrusion and heat transfer in the lower crust: a SHRIMP U/Pb zircon study in the Ivrea-Verbano Zone (Western Alps, Italy). J. Petrol. 48, 1185–1218. https://doi.org/10.1093/petrology/egm014.
Petri, B., Wijbrans, J.R., Mohn, G., Manatschal, G., Beltrando, M., 2023. Thermal evolution of Permian post-orogenic extension and Jurassic rifting recorded in the Austroalpine basement (SE Switzerland, N Italy). Lithos, 444–445. https://doi.org/10.1016/j.lithos.2023.107124.

Pin, C., Monchoux, P., Paquette, J.-L., Azambre, B., Wang, R.C., Martin, R.F., 2006. Igneous albitite dikes in orogenic lherzolites, Western Pyrénées, France: A possible source for corundum and alkali feldspar xenocrysts in basaltic terranes. II. Geochemical and petrogenetic considerations. *Can. Mineral.* 44, 843–856. https://doi.org/10.2113/gscanmin.44.4.843.

Plank, T., 2014. The chemical composition of subducting sediments. In: Holland, H. D. (Ed.), Treatise on Geochemistry. 2nd ed. Elsevier, Amsterdam, pp. 607–629.

Ridolfi, F., Zanetti, A., Renzulli, A., Perugini, D., Holtz, F., Oberti, R., 2018. AMFORM, a new mass-based model for the calculation of the unit formula of amphiboles from electron microprobe analyses. Am. Miner. 103, 1112–1125. https://doi.org/10.2138/am-2018-6385.

Roeder, P., Gofton, E., Thornber, C., 2006. Cotectic proportions of olivine and spinel in olivine-tholeiitic basalt and evaluation of pre-eruptive processes. J. Petrol. 47, 883–900. https://doi.org/10.1093/petrology/egi099.

Roeder, P.L., Poustovetov, A., Oskarsson, N., 2001. Growth forms and composition of chromian spinel in MORB magma: diffusion-controlled crystallization of chromian spinel. Can. Mineral. 39, 397–416. https://doi.org/10.2113/gscanmin.39.2.397.

Salters, V.J.M., Stracke, A., 2004. Composition of the depleted mantle. Geochem. Geophys. Geosys. 5. https://doi.org/10.1029/2003GC000597.

Schaltegger, U., Ulianov, A., Müntener, O., Ovtcharova, M., Peytcheva, I., Vonlanthen, P., Vennemann, T., Antognini, M., Girlanda, F., 2015. Megacrystic zircon with planar fractures in miaskite-type nepheline pegmatites formed at high pressures in the lower crust (Ivrea Zone, southern Alps, Switzerland). Am. Mineral. 100, 83–94. https://doi.org/10.2138/am-2015-4773.

Schettino, A., Turco, E., 2011. Tectonic history of the western Tethys since the Late Triassic. GSA Bull. 123, 89–105. https://doi.org/10.1130/B30064.1.

Schmid, S.M., 1993. Ivrea zone and adjacent southern Alpine basement, *in* von Raumer, J.F., and Neubauer, F., eds., Pre-Mesozoic Geology in the Alps. Springer–Verlag, Berlin, 567–583. https://doi.org/10.1007/978-3-642-84640-3_33.

Selverstone, J., Sharp, Z.D., 2011. Chlorine isotope evidence for multicomponent mantle metasomatism in the Ivrea Zone. Earth Planet. Sci. Lett. 310, 429–440. https://doi.org/10.1016/j.epsl.2011.08.034.

Siena, F., Coltorti, M., 1989. The petrogenesis of a hydrated mafic-ultramafic complex and the role of amphibole fractionation at Finero (Italian Western Alps). Neues Jahrb. Mineral. Monatsh.. 6, 255–274.

Søager, N., Portnyagin, M., Hoernle, K., Holm, P.M., Hauff, F., Garbe-Schönberg, D., 2015. Olivine major and trace element compositions in Southern Payenia basalts, Argentina: Evidence for pyroxenite–peridotite melt mixing in a back-arc setting. J. Petrol. 56, 1495–1518. https://doi.org/10.1093/petrology/egv043.

Soder, C.G., Romer, R.L., 2018. Post-collisional potassic-ultrapotassic magmatism of the Variscan orogen: Implications for mantle metasomatism during continental subduction. J. Petrol. 59, 1007–1034. https://doi.org/10.1093/petrology/egy053.

Stähle, V., Frenzel, G., Hess, J.C., Saupé, F., Schmidt, S.T., Schneider, W., 2001. Permian metabasalt and Triassic alkaline dykes in the Northern Ivrea Zone: clues to the post-Variscan geodynamic evolution of the Southern Alps. Schweizerische Mineralogische Petrographische Mitteillungen 81, 1–21.

Stälhe, V., Frenzel, G., Kober, B., Michard, A., Puchelt, H., Schneider, W., 1990. Zircon syenite pegmatites in the Finero peridotite (Ivrea Zone): evidence for a syenite from a mantle source. Earth Planet. Sci. Lett. 101, 196–205. https://doi.org/10.1016/0012-821X(90)90153-O.

Stampfli, G.M., Borel, G.D., 2002. A plate tectonic model for the Paleozoic and Mesozoic constrained by dynamic plate boundaries and restored synthetic oceanic isochrones. Earth Planet. Sci. Lett. 196, 17–33. https://doi.org/10.1016/S0012-821X(01)00588-X.

Stampfli, G.M., Borel, G.D., 2004. The TRANSMED transects in space and time: Constraints on the paleotectonic evolution of the Mediterranean domain. In: Cavazza, W., Roure, F., Spakman, W., Stampfli, G.M., Ziegler, P. (Eds.), The TRANSMED Atlas: the Mediterranean Region from Crust to Mantle. Springer-Verlag, pp. 53–80.

Stampfli, G.M., Von Raumer, J.F., Borel, G.D., 2002. Paleozoic evolution of pre-Variscan terranes: from Gondwana to the Variscan collision, *in* Catalan, J.R.M., Hatcher, R.D., Arenas, R., Garcia, F.D., eds., Variscan-Appalachian dynamics: The building of the late Paleozoic basement. GSA Special Paper 364, 263–280. https://doi.org/10.1130/0-8137-2364-7.263.

Stampfli, G., Kozur, H., 2006. Europe from the Variscan to the Alpine cycles. Geol. Soc. London Mem. 32, 57–82. https://doi.org/10.1144/GSL.MEM.2006.032.01.04.

Storck, J.-C., Brack, P., Wotzlaw, J.F., Ulmer, P., 2019. Timing and evolution of Middle Triassic magmatism in the Southern Alps (northern Italy). J. Geol. Soc. 176, 253–268. https://doi.org/10.1144/jgs2018-123.

Stracke, A., 2012. Earth's heterogeneous mantle: A product of convection-driven interaction between crust and mantle. Chem. Geol. 330–331, 274–299. https://doi.org/10.1016/j.chemgeo.2012.08.007.

Stracke, A., Bizimis, M., Salters, V.J., 2003. Recycling oceanic crust: quantitative constraints. Geochem. Geophys. Geosys. 4. https://doi.org/10.1029/2001GC000223.

Tappe, S., Foley, S.F., Jenner, G.A., Heaman, L.M., Kjarsgaard, B.A., Romer, R.L., Stracke, A., Joyce, N., Hoefs, J., 2006. Genesis of ultramafic lamprophyres and carbonatites at Aillik Bay, Labrador: a consequence of incipient lithospheric thinning beneath the North Atlantic Craton. J. Petrol. 47, 1261–1315. https://doi.org/10.1093/petrology/egl008.

Tiepolo, M., 1999. Determinazione sperimentale dei coefficient di distribuzione solido/liquid in anfiboli di mantello: Ruolo del controllo cristallochimica. Unpubl. PhD thesis. Universita di Pavia, 314 p.

van Hinsbergen, D.J.J., Torsvik, T.H., Schmid, S.M., Maţenco, L.C., Maffione, M., Vissers, R.L.M., Gürer, D., Spakman, W., 2020. Orogenic architecture of the Mediterranean region and kinematic reconstruction of its tectonic evolution since the Triassic. Gondwana Res. 81, 79–229. https://doi.org/10.1016/j.gr.2019.07.009.

von Raumer, J.F., Bussy, F., Schaltegger, U., Schulz, B., Stampfli, G.M., 2013. Pre-Mesozoic Alpine basements – Their place in the European Paleozoic framework. GSA Bull. 125, 89–108. https://doi.org/10.1130/B30654.1.

Voshage, H., Hunziker, J.C., Hofmann, A.W., Zingg, A., 1987. A Nd and Sr isotopic study of the Ivrea zone, Southern Alps, N-Italy. Contrib. Mineral. Petrol. 97, 31–42. https://doi.org/10.1007/BF00375212.

Wang, J., Su, B.-X., Robinson, P.T., Xiao, Y., Bai, Y., Liu, X., Sakyi, P.A., Jing, J.-J., Chen, C., Liang, Z., Bao, Z.-A., 2021. Trace elements in olivine: Proxies for petrogenesis, mineralization and discrimination of mafic-ultramafic rocks. Lithos 388–389. https://doi.org/10.1016/j.lithos.2021.106085.

Witt-Eickschen, G., Seck, H.A., Mezger, K., Eggins, S.M., Altherr, R., 2003. Lithospheric mantle evolution beneath the Eifel (Germany): constraints from Sr–Nd–Pb isotopes and trace element abundances in spinel peridotite and pyroxenite xenoliths. J. Petrol. 44, 1077–1095. https://doi.org/10.1093/petrology/44.6.1077.

Woelki, D., Salters, V., Beier, C., Dick, H., Koepke, J., Romer, R., 2023. Shallow recycling of lower continental crust: The Mahoney Seamount at the Southwest Indian Ridge. Earth Planet. Sci. Lett. 602,. https://doi.org/10.1016/j.epsl.2022.117968 117968.

Zanetti, A., Mazzucchelli, M., Rivalenti, G., Vannucci, R., 1999. The Finero phlogopite–peridotite massif: an example of subduction-related metasomatism. Contrib. Mineral. Petrol. 134, 107–122. https://doi.org/10.1007/s004100050472.

Zanetti, A., Mazzucchelli, M., Sinigoi, S., Giovanardi, T., Peressini, G., Fanning, M., 2013. SHRIMP U-Pb zircon Triassic intrusion age of the Finero mafic complex (Ivrea–Verbano Zone, Western Alps) and its geodynamic implications. J. Petrol. 54, 2235–2265. https://doi.org/10.1093/petrology/egt046.

Zanetti, A., Giovanardi, T., Langone, A., Tiepolo, M., Wu, F.Y., Dallai, L., Mazzucchelli, M., 2016. Origin and age of zircon-bearing chromitite layers from the Finero phlogopite peridotite (Ivrea–Verbano Zone, Western Alps) and geodynamic consequences. Lithos 262, 58–74. https://doi.org/10.1016/j.lithos.2016.06.015.

Zheng, Y.-F., 2019. Subduction zone geochemistry. Geosci. Frontiers 10, 1223–1254. https://doi.org/10.1016/j.gsf.2019.02.003.

Zurbriggen, R., 1996. Crustal genesis and uplift history of the Strona-Ceneri zone (Southern Alps). Unpubl. PhD thesis, University of Bern, Switzerland.